NOAA Technical Report ERL 413-AOML 29

Numerical Simulation of Tropical Cyclone Development with Latent Heat Release by the Resolvable Scales II: Propagating Small-Scale Features Observed in the Prehurricane Phase

Stanley L. Rosenthal

October 1980

U.S. DEPARTMENT OF COMMERCE
National Oceanic and Atmospheric Administration
Environmental Research Laboratories

NOAA Technical Report ERL 413-AOML 29

Numerical Simulation of Tropical Cyclone Development with Latent Heat Release by the Resolvable Scales II: Propagating Small-Scale Features Observed in the Prehurricane Phase

Stanley L. Rosenthal

Atlantic Oceanographic and Meteorological Laboratories
National Hurricane Research Laboratory
Coral Gables, Florida

October 1980

U.S. DEPARTMENT OF COMMERCE
Philip M. Klutznick, Secretary

National Oceanic and Atmospheric Administration
Richard A. Frank, Administrator

Environmental Research Laboratories
Boulder, Colorado
Joseph O. Fletcher, Acting Director

CONTENTS

NUMERICAL SIMULATION OF TROPICAL CYCLONE DEVELOPMENT WITH LATENT HEAT RELEASE BY THE RESOLVABLE SCALES II: PROPAGATING SMALL-SCALE FEATURES OBSERVED IN THE PREHURRICANE PHASE

Stanley L. Rosenthal

ABSTRACT. Analysis of axisymmetric numerical simulations of hurricane structure and development reveals that large-amplitude small-scale features develop, but they are controlled by physical processes (particularly the nonlinear feedback of the moist convection onto the vertical stratification) that are more adequately modeled here than in earlier attempts. Analysis also reveals the presence of a mesoscale convective system that has many of the features of propagating multicell squall lines observed both in the tropics and in middle latitudes. The simulation data provide a consistent physical description of the mesoscale system despite the updrafts and downdrafts being, for the most part, only one grid point wide and, thus, severely truncated. Stabilization of the low troposphere by downdrafts and precipitation evaporation as observed in the wake of mesoscale tropical systems occurs in these simulations. The model distinguishes between intermittent, multicell, bubble-like convection and steady, plume-like convection. It is argued that the latter is more likely to be cooperative, in the CISK sense, than the former. In view of this, it is suggested that changes in the type, or mode, of cumulus-scale and mesoscale convection that are not now taken into account in existing cumulus parameterization schemes may be important in subsequent amplification of a larger scale system in which the convection is embedded.

1. INTRODUCTION

Rosenthal (1978) described axisymmetric hurricane simulations with a hydrostatic model in which the latent heat release took place entirely in convective cloud elements that were explicitly resolved on a grid with 20-km horizontal resolution. In these simulations large-amplitude small-scale features grew more slowly than in earlier models and were controlled by very distinct physical processes. Analysis of the small-scale features also revealed the presence of a convective system that, in many ways, resembled multicell severe weather systems and tropical squall lines as described by Houze (1976, 1977), Zipser (1969, 1977), and others.

The simulation data provide a reasonably complete physical description of this convective system. The detail presented here provides the reader with a better understanding of the stability of the convective motions and, hence, a fuller appreciation for the calculations. Thus, this paper may be considered a companion to Rosenthal (1978).

From a different view, the physics of the convective system are in themselves interesting and, apparently, similar to those proposed as important in real squall lines. It is, of course, obvious that great caution must be taken in relating these modeling results to the real atmosphere. The model is hydrostatic and, thus, some physical mechanisms thought to be of importance in real squall lines are not represented. Furthermore, the model is axisymmetric. As pointed out by others (e.g., Lilly, 1975; Moncrief and Miller, 1976; Wilhelmson, 1974; Hane, 1973; Schlesinger, 1975), the two-dimensionality is a severe limitation that must be kept in mind when the results are interpreted. However, the most severe limitation probably results from horizontal truncation error, since most of the updrafts and downdrafts are only one grid point wide.

Despite these limitations, the simulations show a reasonable degree of reality, and the

squall line evolves in a physically consistent and interesting fashion. Whether or not these physics are those of the real atmosphere, they could provide clues for future observational studies.

The cloud system that evolves (despite its larger dimensions and longer time scale) appears to be similar to the intermittent mode of cumulus convection discussed by Ludlam (1963), which is favored by small wind shear and large static instability for moist motions.

In the real atmosphere, convective clouds of the size simulated here (at least 20 km wide) would most likely consist of a number of smaller elements (Ludlam, 1963). However, single clouds of approximately this size have been observed (Browning and Foote, 1976; Browning et al., 1976; Newton and Fankhauser, 1975).

2. SUMMARY OF MODEL DETAILS

Rosenthal (1978) gives a complete description of the model. Only a brief summary is presented here. The equations are written in cylindrical horizontal coordinates. In addition to the usual hydrostatic equations, the model includes predictive equations for water vapor, rain water, and cloud water on the resolvable scales. Autoconversion and collection are modeled according to Kessler (1969). Evaporation of rain water follows Brown (1974). The lateral boundary conditions at the origin are the axisymmetric conditions. Thus, the horizontal wind components vanish there as do the horizontal gradients of all other variables. At the outer lateral boundary, the system is mechanically closed with a "sticky" wall. The horizontal wind components and the gradients of all other variables vanish there.

The overall scheme closely conserves total energy, as verified through numerical integration (Moss and Rosenthal, 1975). The time operator is the Euler-backward method (Matsuno, 1965; Kurihara, 1965). The Euler-backward method provides temporal damping for oscillatory motions. However, the small-scale features in the early portions of the integration show growth and decay characteristics, rather than oscillations. It is easy to show that motions with an exponential time variation are amplified by the Euler-backward method. Thus, the physical mechanisms that stabilize these features not only overcome the physical instability, but damp a small numerical instability as well. Further details are given by Rosenthal (1978).

Air-sea interaction is modeled by Kondo's (1975) wind-stability dependent bulk aerodynamic formulation. Vertical turbulent mixing above the surface layer is calculated from a modified version of the Estoque-Bhumralkar (1969) shear and stability dependent K-theory. In addition to the vertical mixing just described, a dry convective adjustment (Kurihara and Tuleya, 1974) is made when the potential temperature is found to decrease with height.

Lateral mixing follows the formulation used by Anthes (1972). The lateral mixing coefficient is written as the sum of a linear and a nonlinear term,

$$K_H = C_1 + k_0^2 \Delta r^2 |D|. \qquad [1]$$

The second part of the right side of (1) is the nonlinear viscosity introduced by Smagorinsky (1963). Here, k_0 is a dimensionless constant, $|D|$ is the magnitude of the total horizontal deformation, Δr is the radial grid increment, and C_1 is a linear lateral mixing coefficient. In the calculation discussed here, $C_1 = 5 \times 10^3\ m^2\ s^{-1}$ and $k_0 = 0.2$. This value of k_0 is generally accepted in modeling studies and has been used in previous hurricane work (e.g., Kurihara and Tuleya, 1974; Kurihara, 1975). Rosenthal (1978) discussed the role of the lateral mixing term in the hurricane evolution aspect of the simulation. In section 4, we discuss the role of this term relative to the small-scale features that are of interest here.

3. DEVELOPMENT OF VERTICAL MOTION

The model vortex is initially in gradient balance with a maximum tangential wind of 7 m s^{-1} at low levels near a radius of 220 km (fig. 1). Rosenthal (1978) described the development as follows:

> In the very early portions of the integration, surface friction destroys the gradient balance. Frictional inflow develops and forces ascent in the interior of the vortex with the strongest ascent occurring somewhat inside the maximum

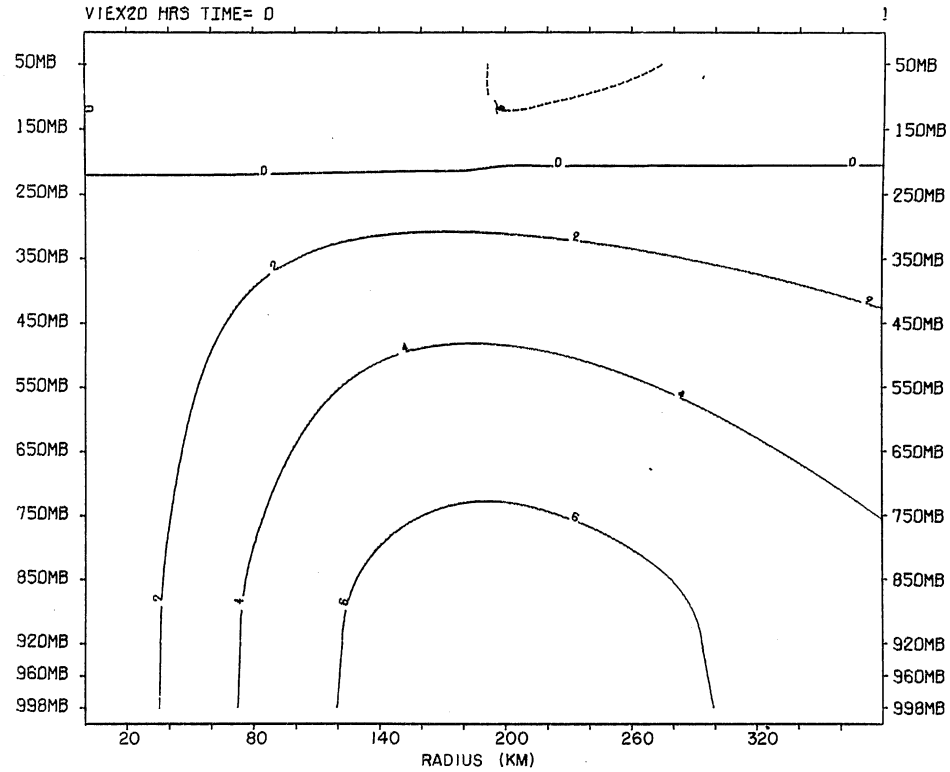

Figure 1.—Vertical cross section of the initial tangential component of the wind (Exp. 20). The vertical axis is labeled with the base-state pressure (mb) corresponding to the various sigma surfaces. Isotachs are drawn at 2 m s^{-1} intervals; negative values are dashed.

tangential wind. [Figure 2] shows the vertical average of $\omega(= dp/dt)$

$$\bar{\omega} = P^{*-1}\int_0^{P^*} \omega \, dp \qquad [2]$$

as a function of time and radius between 3 and 14 h. The figure is constructed from history data at hourly intervals. Condensation first occurs between 9 and 10 h. Thus, the upward motion prior to 10 h is produced entirely by friction. Before condensation starts, only a very slow increase of $\bar{\omega}$ with time is observed. Between 10 and 14 h, as a result of the condensation process, there is a more rapid increase of $\bar{\omega}$ with the maximum remaining, at least during this time interval, at the radius of maximum frictional updraft.

The saturated updraft near 130 km is the parent of the propagating squall-like feature. . . .

[Figure 3] shows the maximum tangential wind as a function of time for the lowest model level ($\sim$150 m) and [figure 4] shows the central pressure (the value of P^* [surface pressure] at 10 km radius) also as a function of time. These graphs are based upon instantaneous values at 12 h intervals. . . . The rapid drop in central pressure that begins at 60 h follows the appearance of an eyelike feature. The tangential wind begins its rapid increase about 12 h earlier.

Figures 5, 6, and 7 show the initial vertical profiles of temperature, relative humidity, and moist static energy at 10-km radius. The sounding is conditionally and convectively unstable below 650 mb. These data are largely (but not entirely) based upon Jordan's (1958) mean hurricane season sounding. The low tropospheric convective instability, as reflected in the moist static energy (fig. 7), is enhanced by the rapid decrease of moisture with height (fig. 6) in the lowest levels.

4. EVOLUTION OF THE CONVECTIVE SYSTEM

4.1 Early Development

By 10:00 h, a thin layer near 920 mb has become saturated (fig. 8) much in the same way as has been observed to precede a case of midlatitude squall-line development (Lewis et al., 1974). Between 10:00 and 15:00 h, the cloud slowly builds upward to 850 mb (fig. 9).

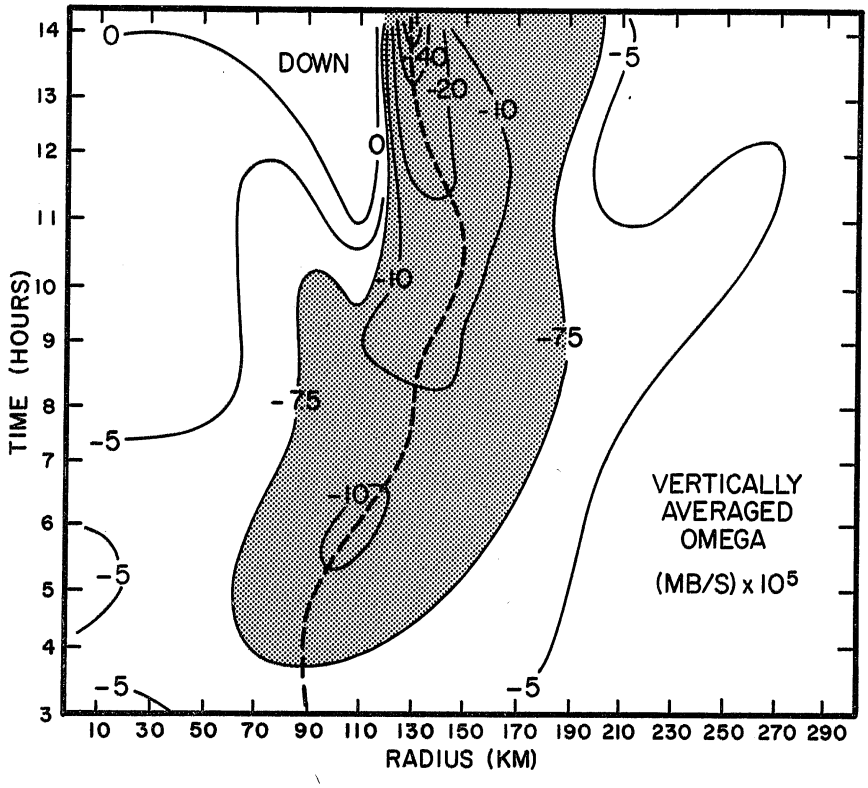

Figure 2.—Time-radius cross section of the vertically integrated $\omega(=dp/dt)$ (Exp. 20). Negative values indicate upward motion. Regions of strongest upward motion are shaded.

At the same time, the vertical motion pattern (fig. 10) narrows and grows vertically. By 15:00 h, the updraft reaches 550 mb but is only saturated from 960 mb to 850 mb. Compensating subsidence is concentrated close to the moist updraft, as predicted by linear theory (Lilly, 1960) and discussed by Fritsch (1975). Because of lateral eddy mixing, a small amount of cloud water evaporates into the subsiding air. However, the thermodynamic effect of this process is negligible, and the compensating subsidence is very nearly a dry adiabatic process. Two other cloud elements (fig. 9), near radii of 190 and 250 km, are soon to dissipate as a result of the subsidence produced by the primary convection. The moist static energy at 15:00 h (fig. 11) shows an upward bulge at 130 km associated with the moist updraft and downward bulges on either side that are produced by the compensating subsidence.

As we shall see in succeeding figures, the configuration at 15:00 h is not maintained for long. The low static energy air, carried downward by the compensating subsidence, will be advected by the cloud circulation into the lower part of the moist updraft. This process, as verified by calculations of the horizontal advection of moist static energy (not shown), is already in progress at 15:00 h. Ultimately, the pocket of high energy air associated with the moist updraft will be cut off from the low layers. The cutoff will consist of thermally buoyant, low-level air with active condensation. This element will rise through vertical advection and leave a layer of stable air in its wake. The higher-level air that produces the cutoff will be dry, and the wake beneath the cutoff will be unsaturated. As the cloud base rises through this process, stable ascent and cooling will occur beneath it. The cooling will be aided by evaporation of precipitation that will fall from the rising cloud. As a result of the cooling beneath the cloud, a hydrostatic pressure rise will occur at low levels and a downdraft will form. The downdraft will start at the lowest levels and build upward to the cloud element. As in the case of the mesoscale downdrafts described by Houze (1976, 1977) and Zipser (1969, 1977), precipitation evaporation will be insufficient to maintain saturation and the downdraft will become warm and dry with time.

The downdraft will be coaxial with the cloud element updraft above it. Coaxial downdrafts, which form at the lowest model level and build upward to the cloud, have been observed in

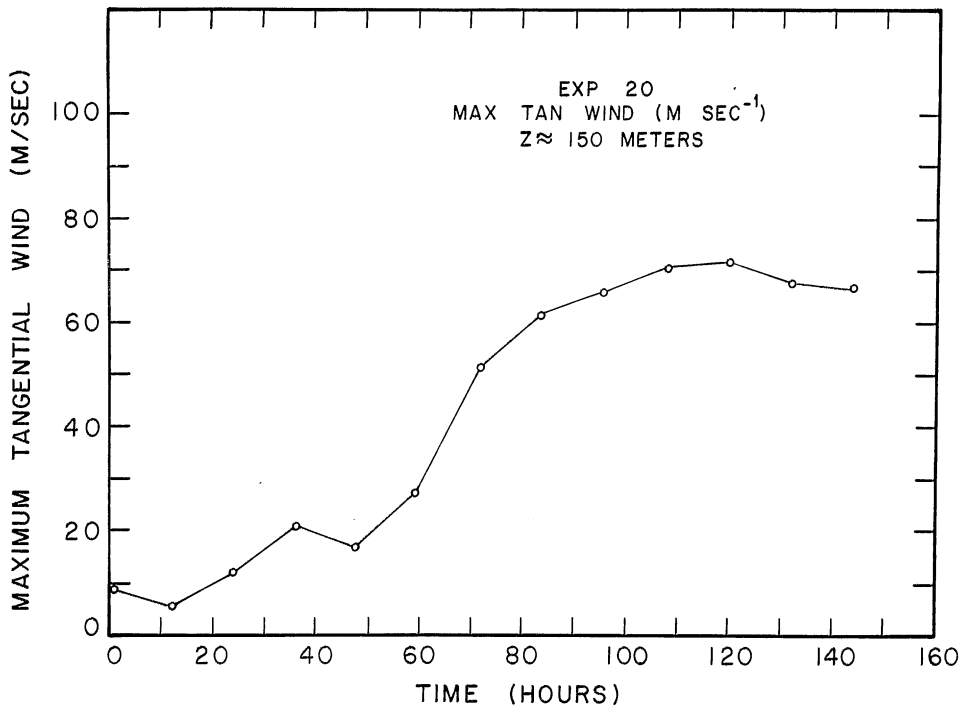

Figure 3.—Maximum tangential wind component (Exp. 20) at the model's lowest wind level as a function of time. Figure is constructed from data at 12-h intervals.

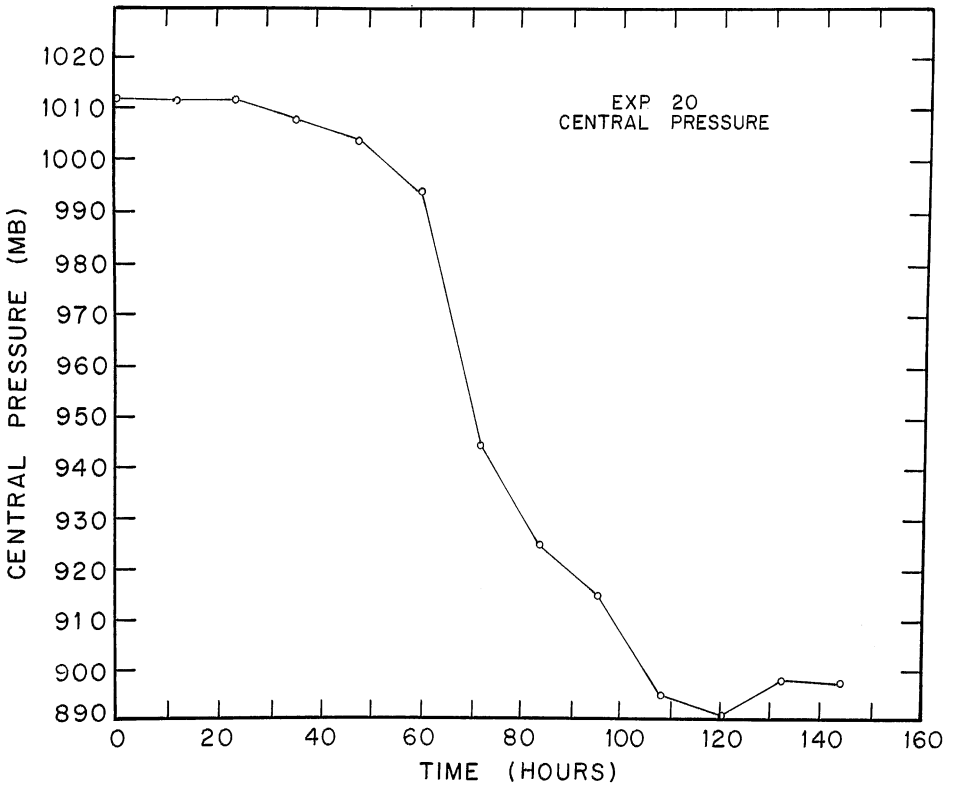

Figure 4.—Central pressure (surface pressure at 10-km radius) as a function of time (Exp. 20). Figure is constructed from data at 12-h intervals.

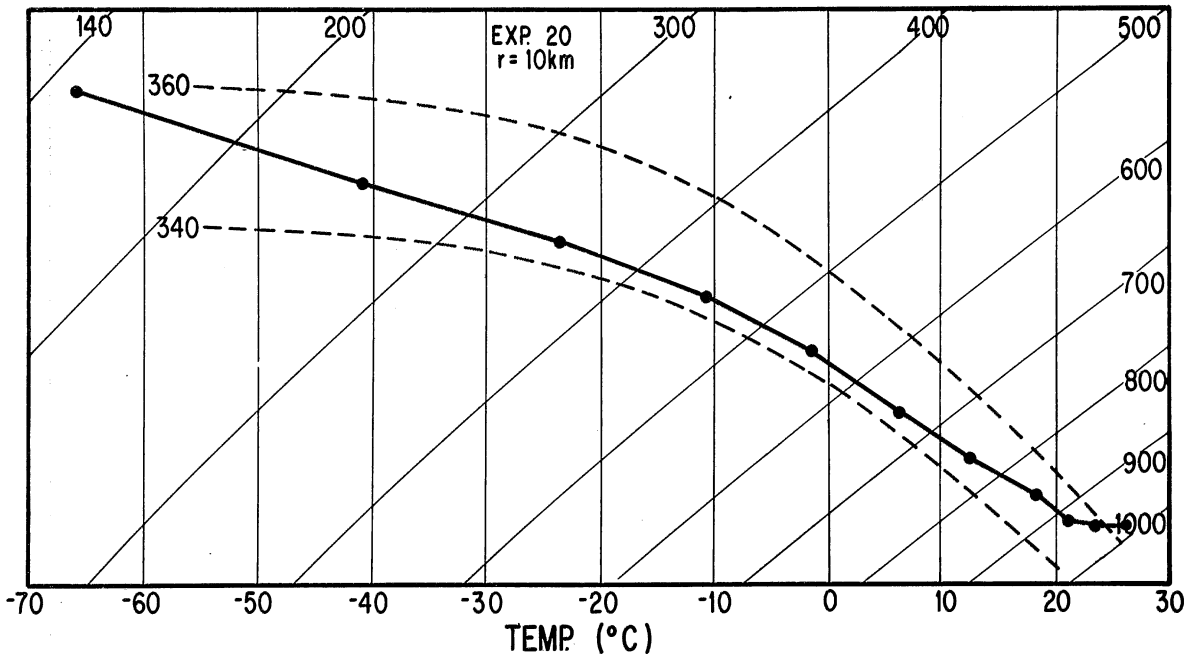

Figure 5.—Initial temperature (Exp. 20) at 10-km radius as function of base-state pressure.

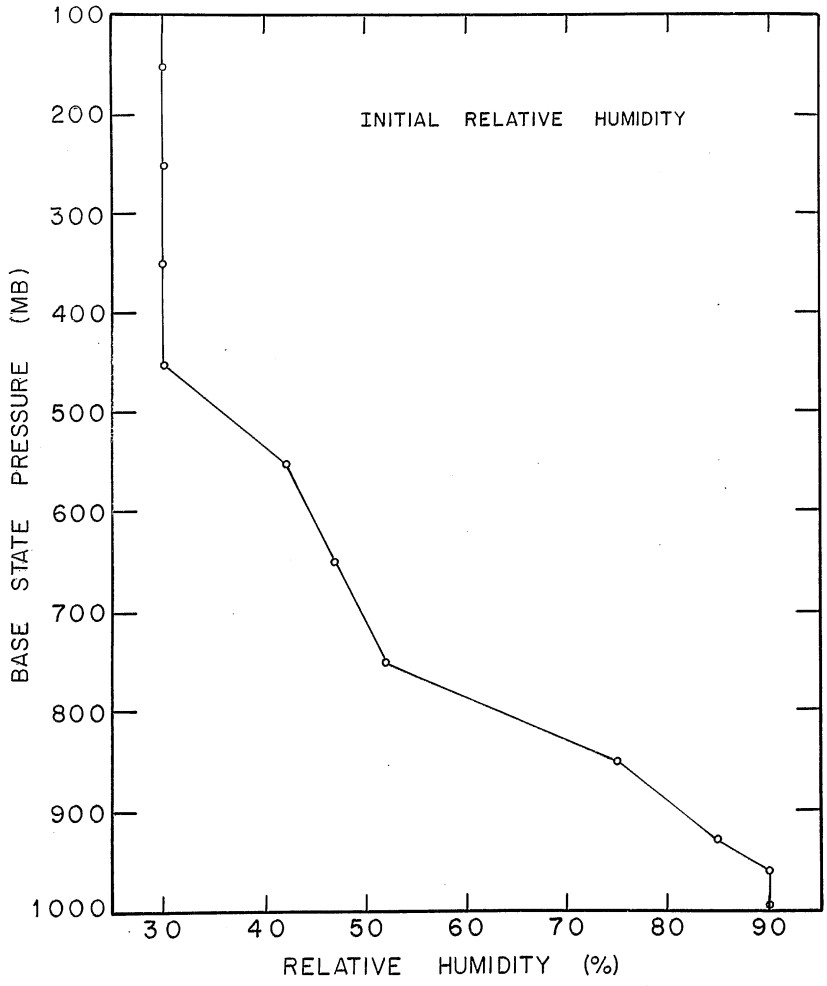

Figure 6.—Initial relative humidity at 10-km radius as a function of base-state pressure (Exp. 20).

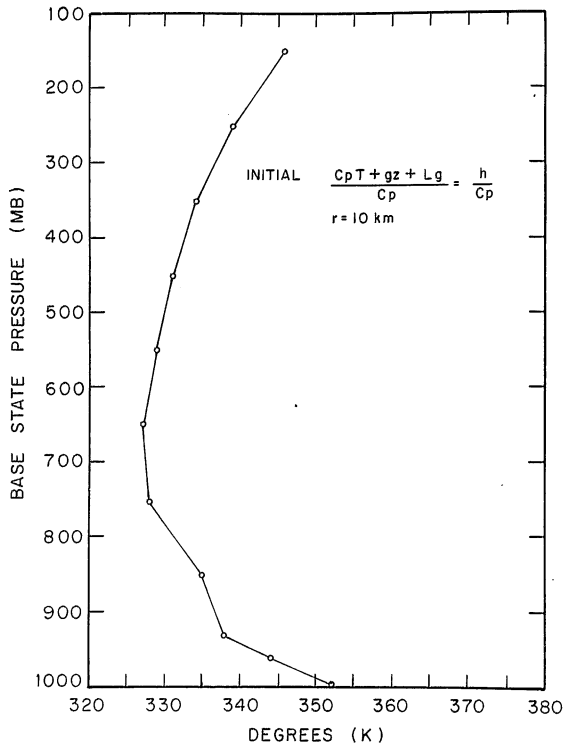

Figure 7.—Moist static energy divided by the specific heat capacity at constant pressure at 10-km radius as a function of base-state pressure (Exp. 20)

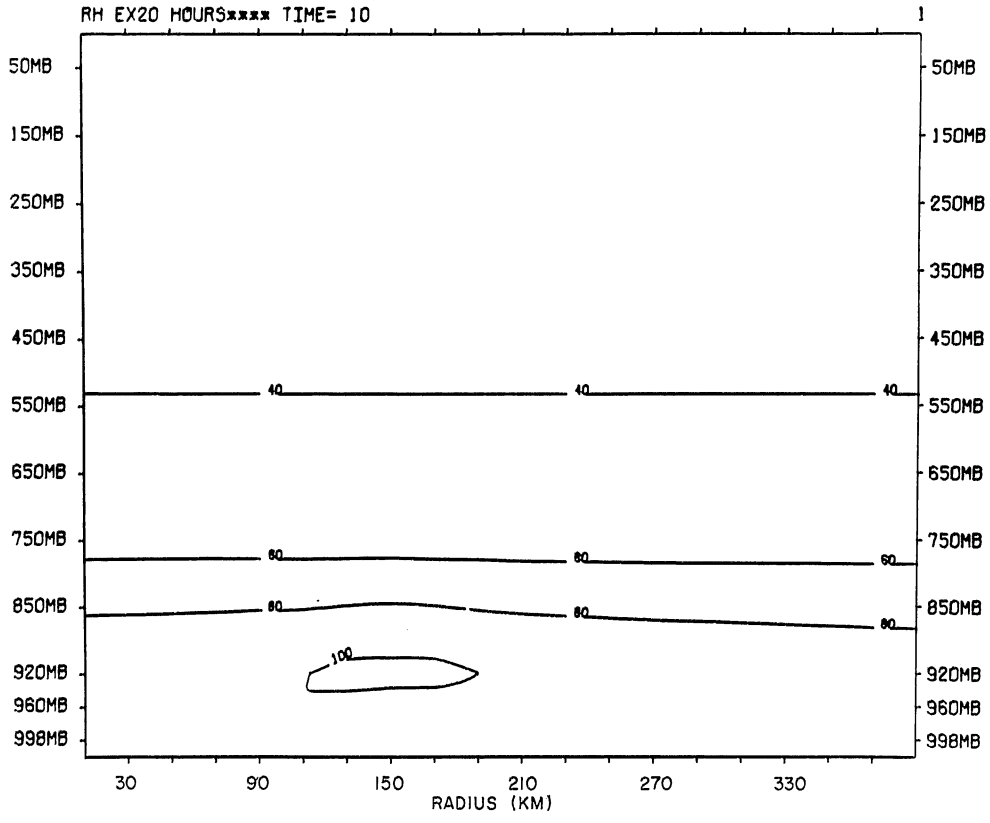

Figure 8.—Vertical cross section of the relative humidity at 10:00 h. Contours are at 20% intervals (Exp. 20).

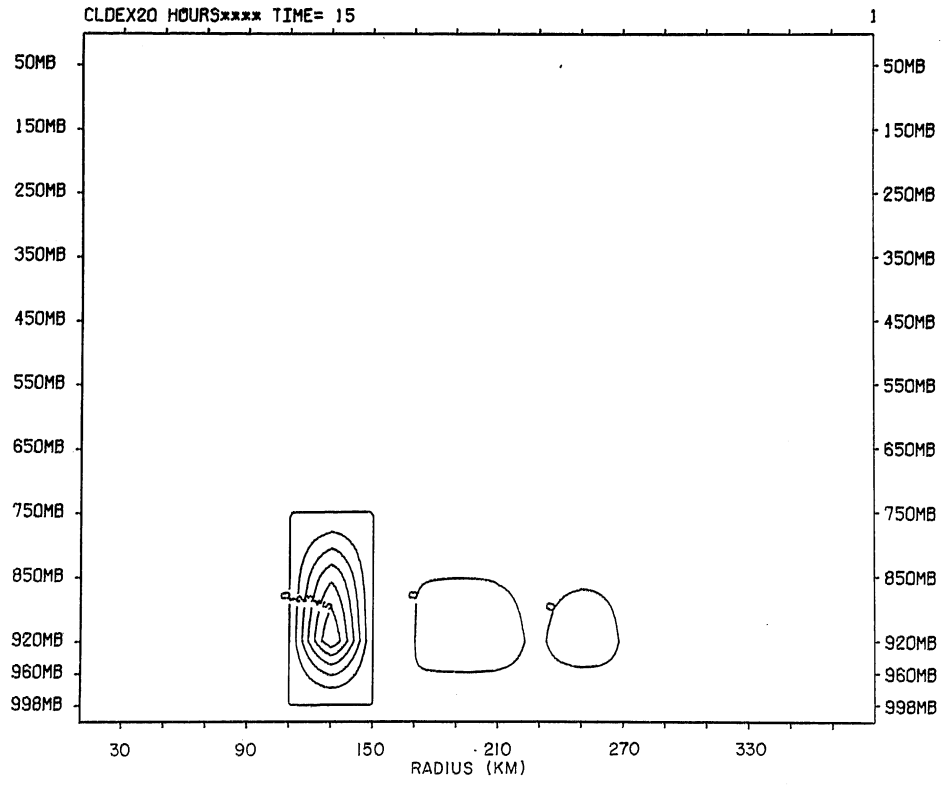

Figure 9.—Vertical cross section of cloud water at 15:00 h. Contours are at intervals of 1 g 10^{-1} kg^{-1} (Exp. 20).

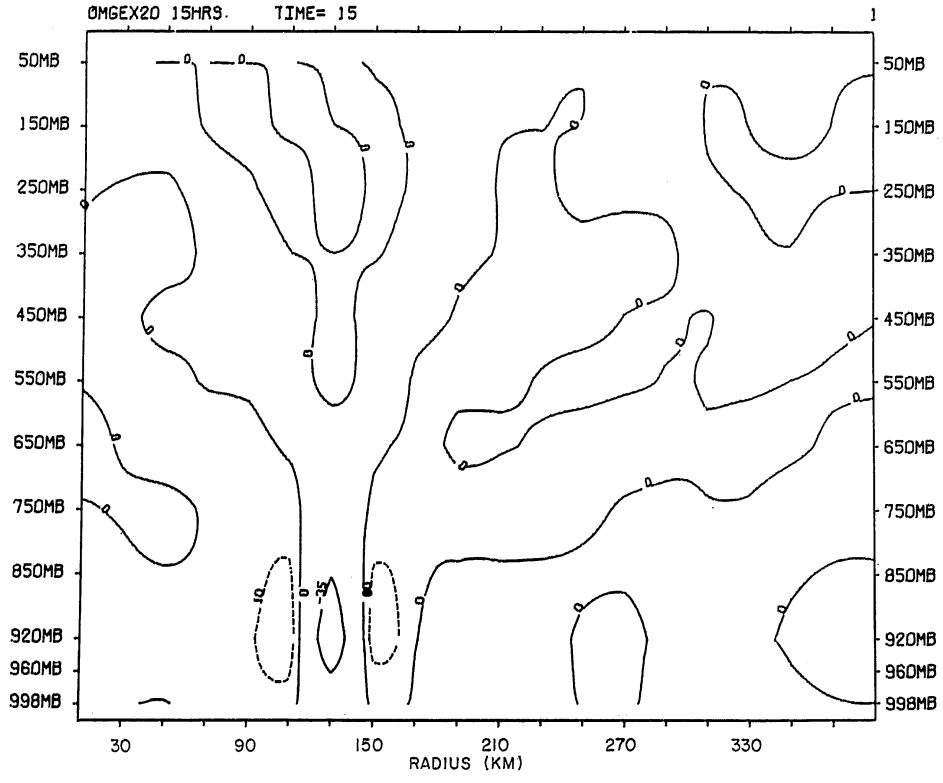

Figure 10.—Vertical cross section of $\omega(=dp/dt)$ at 15:00 h. Units are in mb per hour and contour interval is varied. Downward values are dashed (Exp. 20).

Table 1. Surface pressure departure (mb) from 1012 mb as a function of radius and time (Exp. 20)

Time (h:min)	Radius (km)							
	110	130	150	170	190	210	230	250
15:30	+0.1	0.0	+0.3	+0.6	+0.7	+0.8	+0.9	+1.1
16:00	-0.1	-0.2	+0.1	+0.5	+0.6	+0.8	+0.9	+1.0
16:30	-0.4	-0.2	-0.2	+0.3	+0.6	+0.8	+0.9	+1.0
17:00	-0.7	-0.3	-0.7	-0.1	+0.4	+0.6	+0.8	+1.0
17:30	-0.8	+0.1	-0.9	-0.8	0.0	+0.4	+0.7	+0.9
18:00	-1.0	+0.7	-1.0	-1.3	-0.6	0.0	+0.4	+0.6
18:30	-1.3	-0.6	-1.0	-1.6	-1.4	-0.7	-0.1	+0.3
19:00	-0.1	-3.4	-0.1	-1.8	-2.3	-1.9	-1.4	-0.8
19:30	-3.9	+0.5	+0.4	-0.9	-0.8	-1.2	-1.6	-1.7
20:00	+0.6	-1.9	-3.9	+1.3	-0.5	+0.1	-0.1	-0.4
20:30	-2.0	-0.6	+0.4	+0.5	-0.9	-0.9	0.0	+0.4
21:00	0.0	+1.8	+1.6	-0.8	+0.2	-0.6	-0.7	-0.3
21:30	+0.7	+0.2	-2.8	-0.9	-0.9	+2.3	+0.1	-0.1
22:00	-1.5	-3.0	+0.5	+1.9	-0.5	-0.8	+0.3	+0.2
22:30	0.0	+2.0	+1.5	-1.8	-1.5	+2.5	+0.6	+0.8
23:00	+1.5	+0.5	-0.7	+0.6	+1.9	-0.6	+1.3	+0.7
23:30	-0.1	+0.2	+0.7	+2.1	+1.6	-0.5	+1.9	+1.3
24:00	+0.6	+0.7	+1.6	+2.2	+0.9	-0.6	+1.5	+1.5

previous two-dimensional numerical simulations of clouds in low wind-shear situations (e.g., Schlesinger, 1973; Takeda, 1971). In those cases the authors attributed downdraft development to evaporative cooling and/or precipitation drag. The development of a downdraft from cooling by stable ascent beneath a cutoff convective element appears to be a physical mechanism that has not been previously considered or discussed. Schlesinger's (1973) data indicate that a cutoff of air with relatively high equivalent potential temperature may have taken place before his downdraft formed.

Ludlam (1963) discussed downdraft formation in low-shear and no-shear situations and speculated that pronounced downdrafts could be produced in these situations only if the convection is intermittent so that the updraft consists of a succession of thermals. In such a situation, Ludlam (1963) suggested that downdrafts would be produced as a result of precipitation evaporation into midlevel air with low equivalent potential temperature. The convection that develops in this simulation behaves much like a succession of thermals, and precipitation evaporation into air with low moist static energy does occur beneath the thermals. However, as we verify later, ascent of stable air is the dominant cooling mechanism leading to formation of the first downdraft.

While the processes leading to downdraft formation are in progress, compensating subsidence, on either side of the original moist updraft (fig. 10), will warm the atmosphere and hydrostatically lower the pressure sufficiently at low levels to reverse the direction of the vertical motion. The region of ascent will, therefore, broaden at its bottom; ultimately air on either side of the original cloud will reach its condensation level, and two new clouds will form. The development of new cloud elements on either side of a saturated updraft has also been observed in previous two-dimensional simulations with low-shear conditions (Takeda, 1971). Hoxit et al. (1976) emphasized the role of subsidence in producing surface pressure falls and low-level convergence ahead of existing convection. In the cases they considered, shear and high tropospheric subsidence were of primary concern. Despite these differences, however, subsidence warming plays a major role in the development, organization, and maintenance of the systems studied here.

The data at 16:30 h (fig. 12) show the cloud element cut off from the boundary layer. Convective stability is present between 920 and 850 mb, and unsaturated air is present at 920 mb. Cooling is evident (fig. 13) near 920 mb. Ascent (fig. 14) continues through the stable layer. The warm pocket (fig. 13) at 130 km and 850 mb reflects the location of the cut-off, low-level air. The lobes that protrude from either side of the warm air have been produced by subsidence. The lower portion of the updraft (fig. 14) has started to broaden. The cool pocket (fig. 13) near 700 mb, above the cloud element, is produced partly by evaporation and partly by adiabatic expansion as the ascent extends to higher levels than does the cloud. The cool air (fig. 13) at the lowest

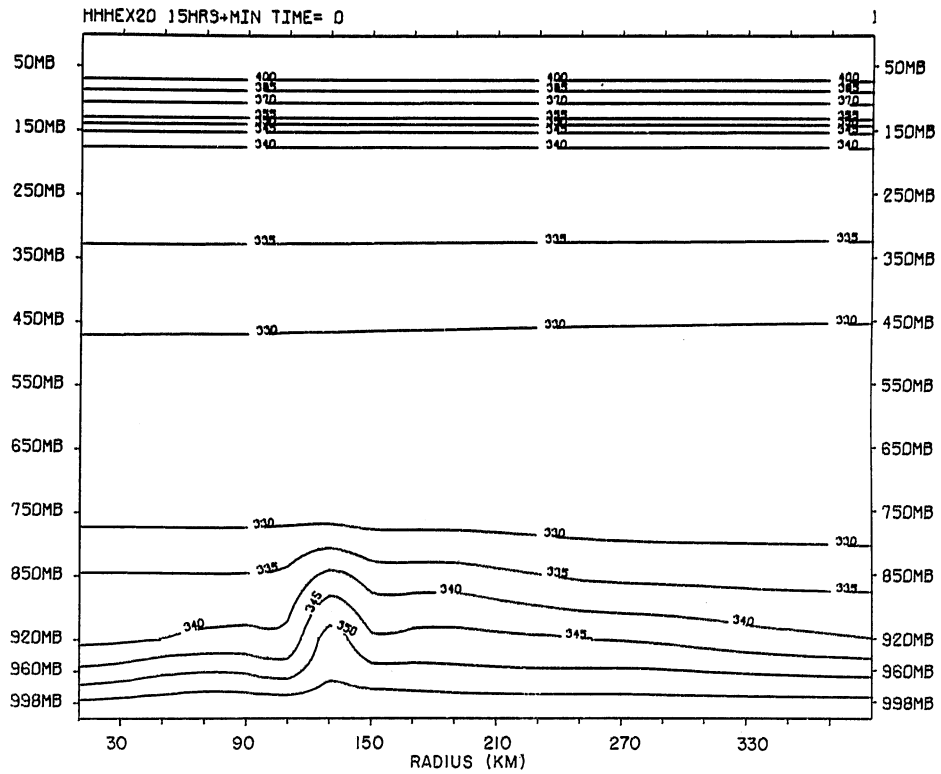

Figure 11.—Vertical cross section of moist static energy divided by the specific heat capacity at constant pressure for dry air at 15:00 h. Values are in kelvin. Contour interval is varied in the upper levels (Exp. 20).

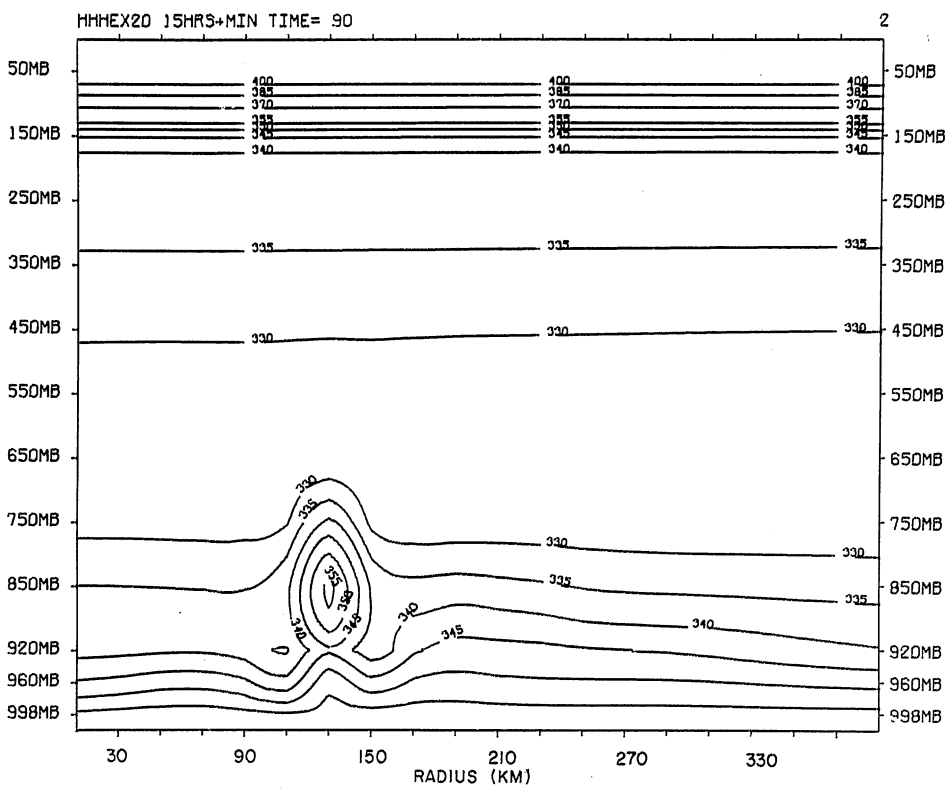

Figure 12.—Vertical cross section of moist static energy at 16:30 h (Exp. 20).

Table 2. Divergence of the surface pressure-gradient force in units of 10^{-5} s^{-1} h^{-1} as a function of radius and time (Exp. 20)

Time (h:min)	Radius (km)							
	110	130	150	170	190	210	230	250
15:30	10.3	-42.3	11.1	7.3	-0.2	0.6	0.2	0.8
16:00	-9.3	-21.8	-11.0	16.0	1.9	1.2	0.3	1.0
16:30	-31.9	17.8	-46.4	22.5	7.3	2.1	0.5	1.3
17:00	-43.0	65.7	-80.4	12.9	18.4	4.5	0.5	1.8
17:30	-23.1	142.8	-80.9	-49.4	26.9	9.4	3.2	2.0
18:00	-88.1	254.3	-98.0	-80.9	8.3	17.8	7.3	2.8
18:30	-36.6	89.4	8.2	-57.5	-38.3	10.3	10.1	8.3
19:00	343.8	-501.1	380.4	-94.4	-65.8	-10.9	-2.5	-0.8
19:30	-457.1	338.1	92.5	-110.7	36.8	6.3	-23.6	-33.2
20:00	283.1	-37.5	-539.2	527.4	-184.1	46.5	32.9	-5.8
20:30	-286.0	27.7	68.9	116.4	-111.5	-59.0	27.2	39.2
21:00	30.3	155.6	158.0	-248.2	129.1	-47.3	-38.9	-9.1
21:30	141.6	193.6	-373.5	-95.2	400.6	-146.8	1.6	-25.7
22:00	38.7	-370.1	148.3	287.0	-273.6	136.9	-34.5	6.1
22:30	-148.6	185.1	209.4	-270.0	-277.9	448.1	-160.9	9.1
23:00	226.4	19.3	-192.6	2.4	193.1	-153.1	101.9	-63.7
23:30	-111.6	-24.2	-62.2	144.9	38.0	-178.9	146.5	-30.9
24:00	34.4	-54.1	-22.3	141.9	-77.3	-92.7	69.3	34.6

level is produced by precipitation evaporation (not shown) and ascent. Tables 1 and 2 show that the surface pressure-gradient force at 130 km is already divergent and verify that convergent surface pressure-gradient forces are present at 110 and 150 km.

At 17:20 h the downdraft (fig. 15) has started to form. The lower part of the updraft has broadened dramatically and new vertical velocity maxima are present at the 110- and 150-km radii. The vertical velocity at 150 km is somewhat stronger and a new cloud element (fig. 16) has already formed there. The moist static energy (fig. 17) shows the original cloud element to be completely detached from the lowest layers. Its center, near 750 mb, is very nearly coincident with the vertical velocity maximum. The upward bulge, at 150-km radius, of the contours of moist static energy is associated with the new cloud element. The base of the original cloud (fig. 16) is now at 850 mb. Compensating subsidence will soon lead to the formation of a convergent surface pressure-gradient force (table 2) and a new updraft at 170 km.

Precipitation (fig. 18) is falling from the center of the original cloud element, and precipitation evaporation occurs at all levels below 850 mb. The temperature anomalies (fig. 19) are similar in pattern to those at 16:30 h (fig. 13), but with increased intensity and horizontal scale. Between 750 and 850 mb there is ascent of convectively stable air (figs. 15 and 17). At 920 mb there is unsaturated ascent. The radial motion (not shown) indicates that the new cloud at 150 km is fed by undilute boundary-layer air from the vortex's exterior. However, much of the ascent in the new updraft at 110 km consists of higher-level air that has descended in the downdraft beneath the original cloud.

Further discussion will be facilitated through the introduction of nomenclature for identification of cloud elements and cloud-produced cold downdrafts. Cloud elements are identified by CXXX where XXX is the radius in kilometers at which the cloud formed. The first cloud is then C130 and the second is C150 (fig. 16). The cold downdrafts are coded as DXXX so that the downdraft forming at 130 km is D130.

At 17:20 h the updraft-downdraft configuration (fig. 15) is not yet fully developed. As the system reaches maturity, it will begin to propagate radially outward through a generation-decay process that, despite the absence of significant wind shear, resembles the propagation of observed tropical squall lines as described by Houze (1976, 1977) and Zipser (1969, 1977). The process is also very much like that by which midlatitude multicell severe storms propagate (Browning et al., 1976). Because of compensating subsidence as well as downdraft outflow, new clouds form radially outward from older ones. In most cases, new clouds also form radially inward of the system. The clouds forming on the outer flank of the system, however, have access to the unprocessed, energy-rich, boundary-layer air from the exterior and they are, therefore, the dominant ones. While new cloud development is in progress, older clouds are cut off to the

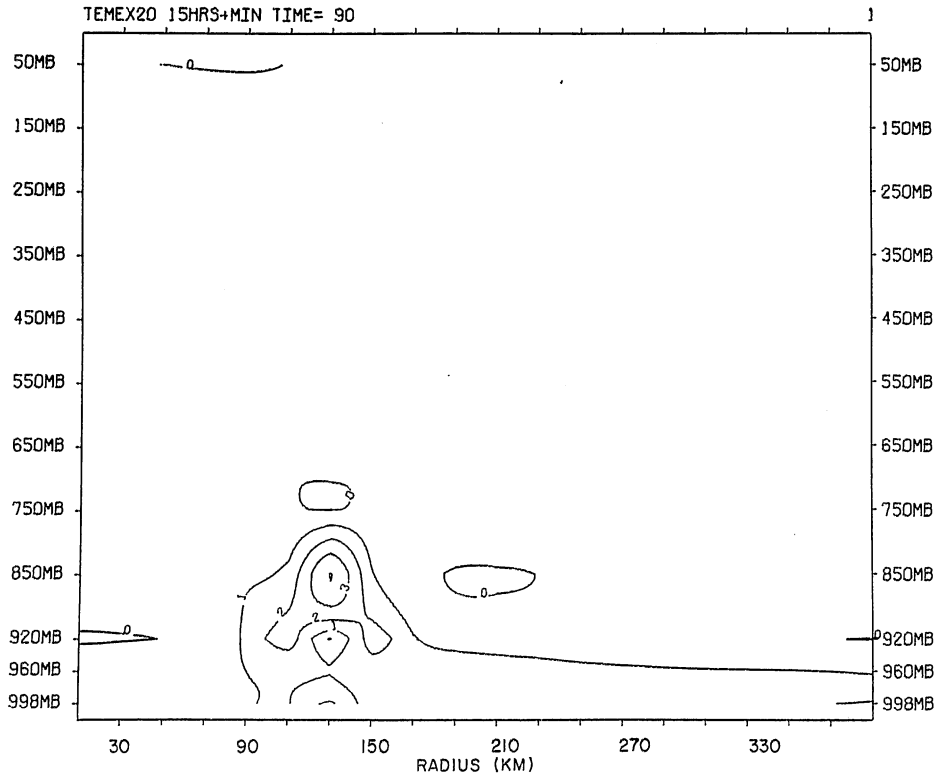

Figure 13.—Vertical cross section of temperature (K) departures (anomalies) from the base state at 16:30 h. Contour interval is 1 K (Exp. 20).

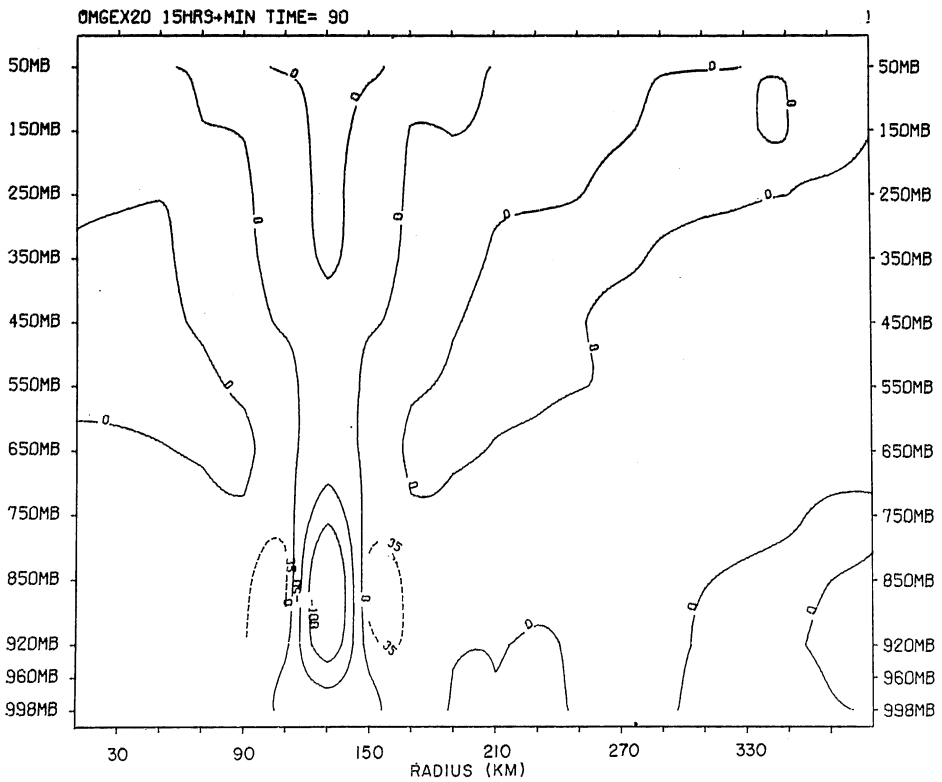

Figure 14.—Vertical cross section of ω at 16:30 h (Exp. 20).

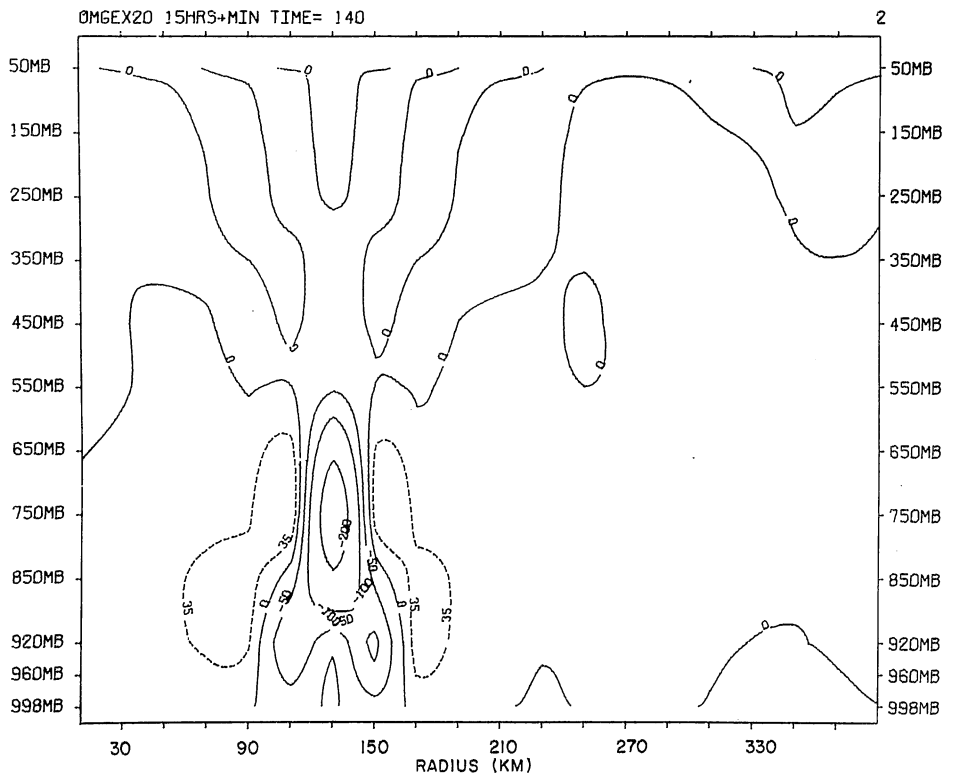

Figure 15.—Vertical cross section of ω at 17:20 h (Exp. 20).

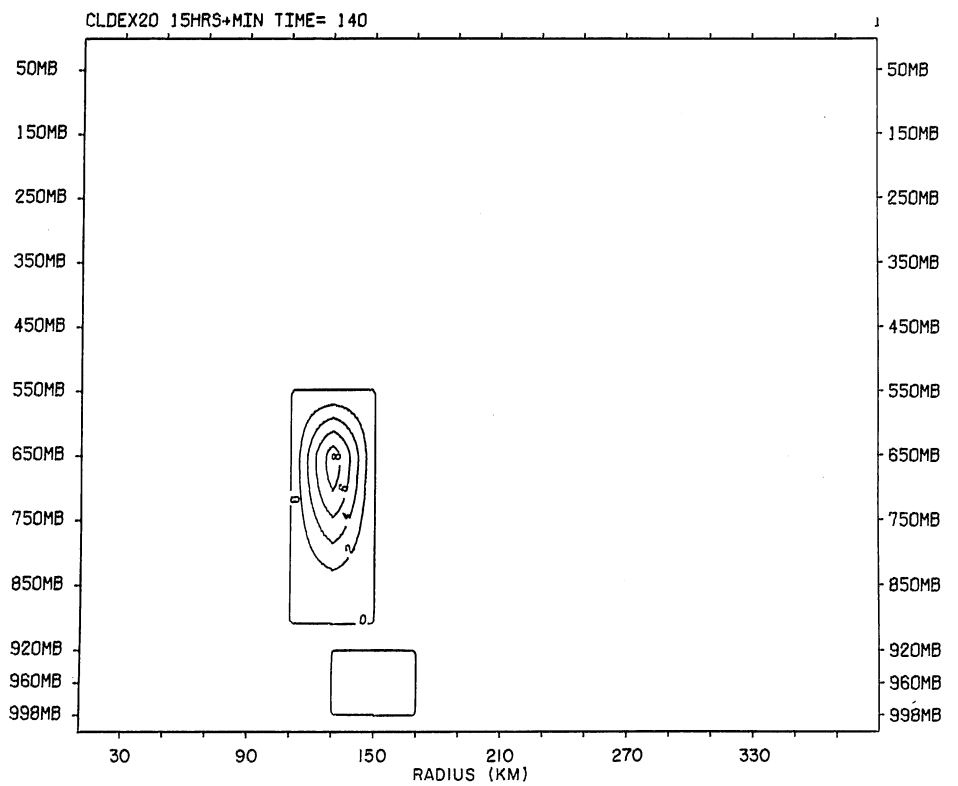

Figure 16.—Vertical cross section of cloud water at 17:20 h. Contour interval is 2 g 10^{-1} kg^{-1} (Exp. 20).

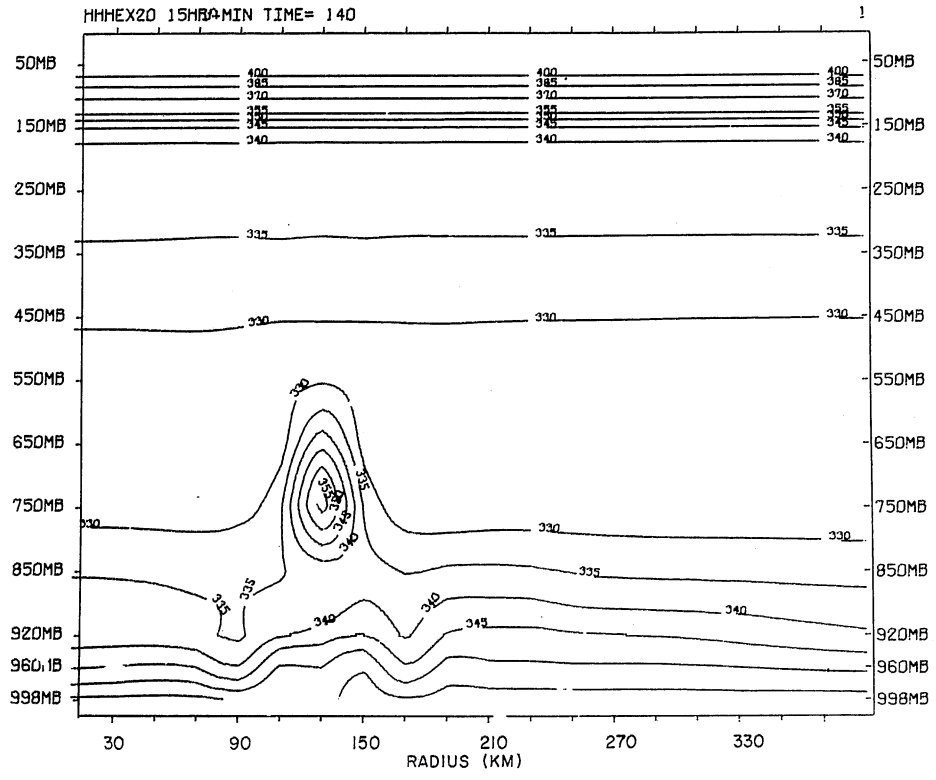

Figure 17.—Vertical cross section of moist static energy at 17:20 h. (Exp. 20).

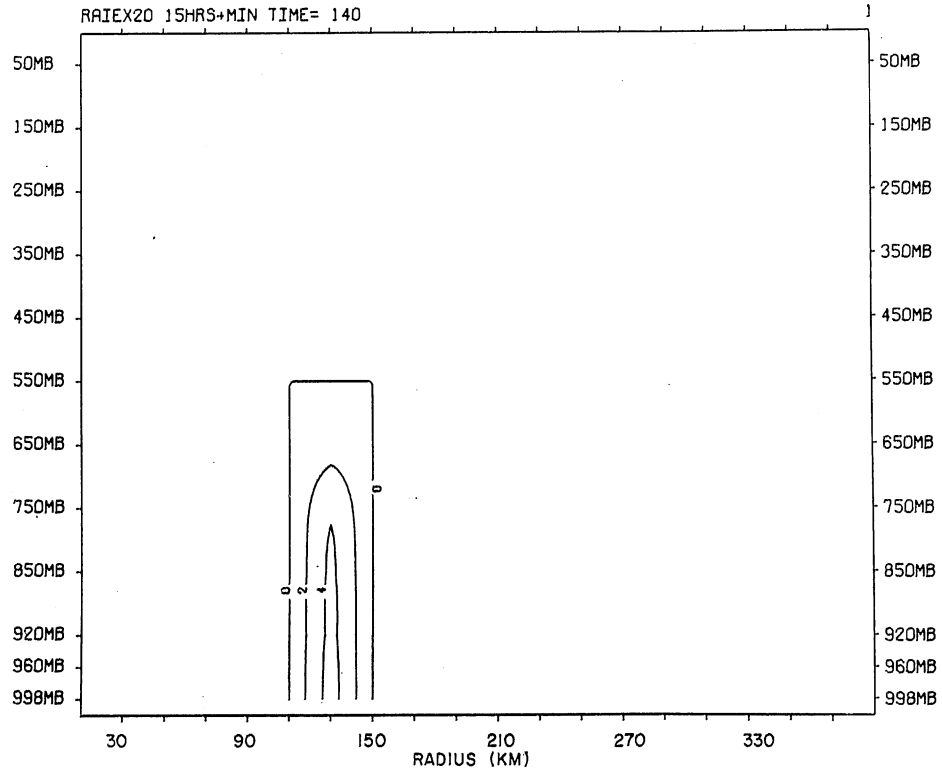

Figure 18.—Vertical cross section of rain water at 17:20 h. Contour interval is 2 g 10^{-1} kg^{-1} (Exp. 20).

rear in much the same way as was the case for C130. The cutoff and its attendant layer of convectively stable air set the stage for new cooling and for new downdraft formation. Older downdrafts, such as D130, become warm and dry because of their unsaturated descent, and ultimately they decay. The net effect of these processes is an outward propagation of the convection. This propagation, however, occurs in discrete steps rather than through the motion of individual cloud elements. The cloud elements, while they are buoyant, behave like unstable gravity waves and, since there is no broad-scale current, have no horizontal motion. Newton and Fankhauser (1975) have emphasized the discrete propagation of midlatitude multicell systems. Houze (1976, 1977) has shown, through detailed analysis of radar data, that a tropical squall that moved through the GATE radar array also propagated in discrete steps.

At 18:00 h, we see continued development of the vertical motion system (fig. 20). The updraft associated with C150 has become wider in its lower portions, while the C110 updraft has broadened through its entire depth. Both changes are produced by subsidence warming that is clearly evident in the temperature anomalies (fig. 21) and the surface pressure-gradient force (table 2). The moist static energy (fig. 22) shows that air whose origin is between 750 and 850 mb is cut off below 850 mb in D130. Boundary-layer air is very nearly cut off in C150. Air entering the very lowest layer of the column at 150-km radius is downdraft air from D130. However, at 920 mb, the air entering C150 is warm and dry and has come to low levels in compensating subsidence at 170 km. This differential horizontal advection is clearly shown in time cross sections of radial motion and of moist static energy advection (not shown).

As a result of this differential advection, the lowest layers of the updraft at 150 km are cooled by horizontal advection, an effect that did not come into play in the evolution of C130 and D130. The effect of this low-level cooling is twofold. On the one hand, it contributes toward a relative low-level hydrostatic pressure increase below C150. The immediate result of this is to tend to weaken the upward motion at that location. On the other hand, convergence is accelerated radially outward from the cooling. Thus, the low-level cooling from horizontal advection of downdraft air tends to control and brake the growth of C150 and, at the same time, to aid in the development of C170. This effect is not of great importance relative to C150 and C170, but it becomes progressively more important with later cloud elements. The process appears to be a crude simulation of the action of thunderstorm outflows in the generation of new convection that, in turn, provides for an organized motion of some tropical mesoscale systems, as indicated by Moncrief and Miller (1976), Zipser (1977) and others.

Significant cloud water (fig. 23) is present in C110 and C150, and precipitation (not shown) is reaching the surface from both clouds. However, the heaviest surface rainfall continues to have its source in C130. The relative humidity at 18:00 h (not shown) in D130 is less than 80% at 920 mb.

The data at 18:00 h show the first updraft-downdraft configuration in a well-developed state. Precipitation evaporation has contributed to cooling of subcloud air and to the development of C150 and C110. However, the dominant mechanisms in developing the vertical motion patterns have been the compensating subsidence and the subsequent recycling of this air into the lower portion of the moist updraft that produced the cutoff of C130 and the stable layer below it. This was verified by Exp. 15 in which the microphysical processes were suppressed and condensate was removed from the system immediately upon its formation. Otherwise, Exp. 15 was identical to Exp. 20.

Figures 24, 25, and 26 show vertical motion, moist static energy, and temperature anomalies at 18:20 h (Exp. 15). The vertical motion and moist static energy are qualitatively similar to those of Exp. 20 at 18:00 h. Only the temperature patterns (figs. 21 and 26) show significant differences. Without evaporation, we do not find cooling in the lowest layers. Beyond this point, however, the two experiments evolve in vastly different ways. The convective system in Exp. 15 degenerates into a series of standing gravity oscillations. Comparisons between the two experiments clearly reveal the important role played by evaporation in forming low-level cold air and the role played by that air in initiating new cloud growth and thereby providing for the propagation and long life of the mesoscale system. The influence of evaporation in stabilizing the lowest levels (and thereby determining the

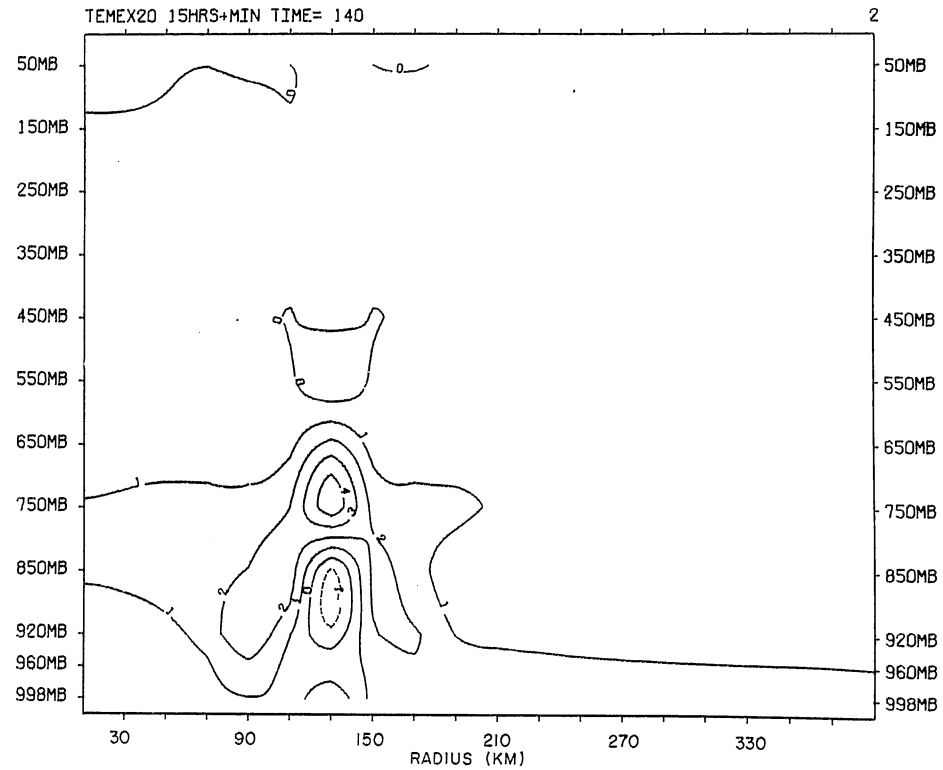

Figure 19.—Vertical cross section of temperature anomaly at 17:20 h. Negative values are dashed (Exp. 20).

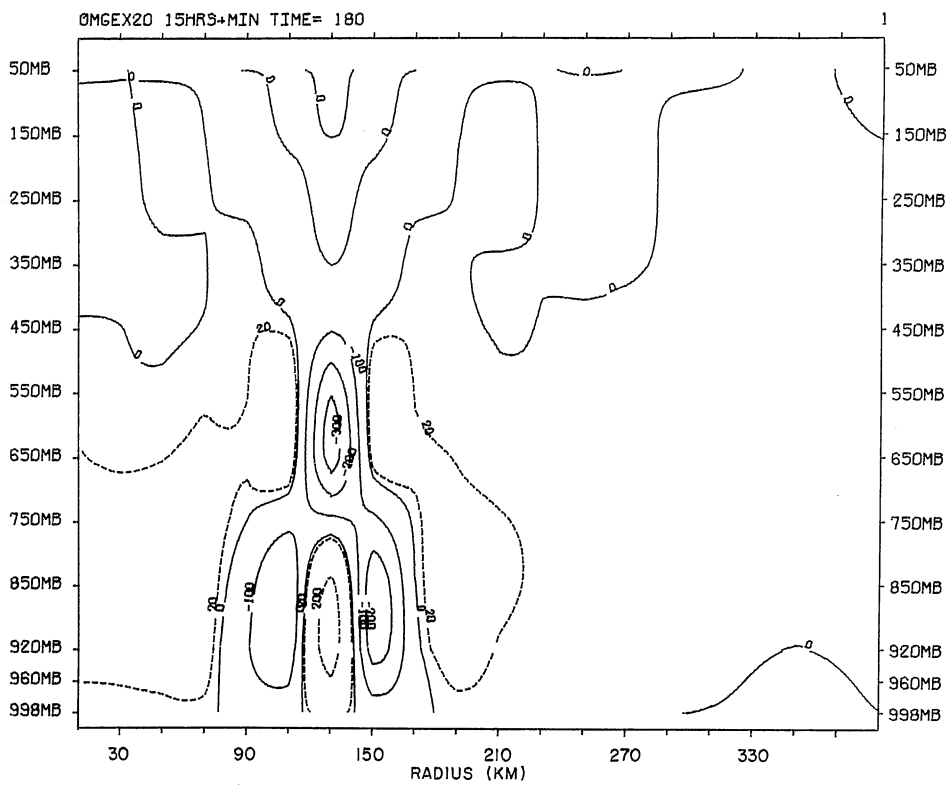

Figure 20.—Vertical cross section of ω at 18:00 h (Exp. 20).

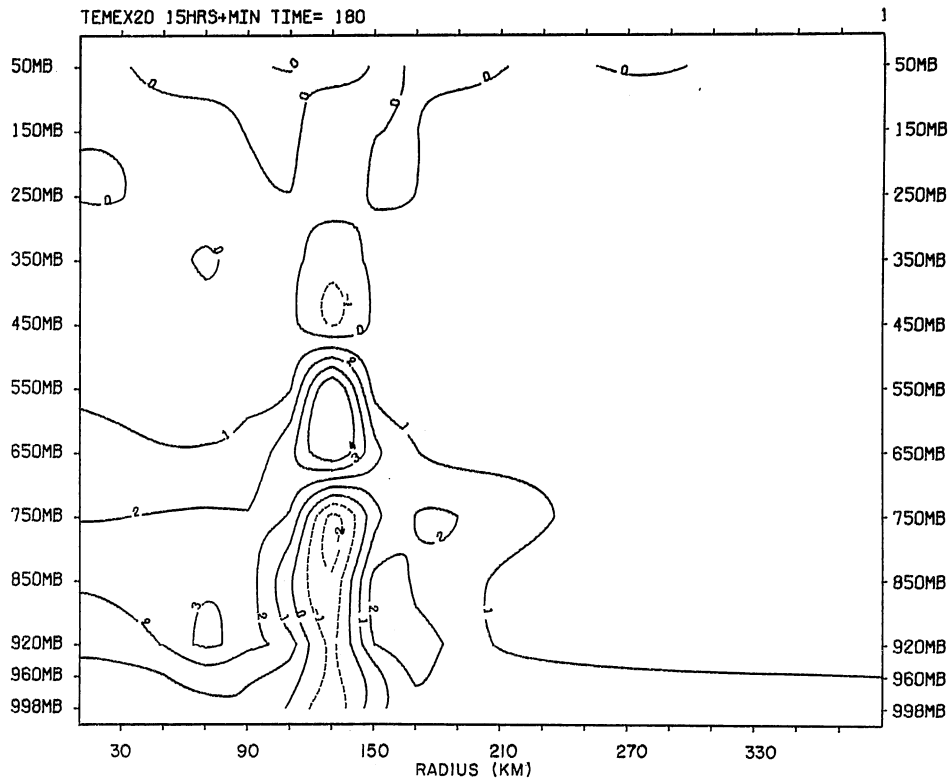

Figure 21.—Vertical cross section of temperature anomaly at 18:00 h (Exp. 20).

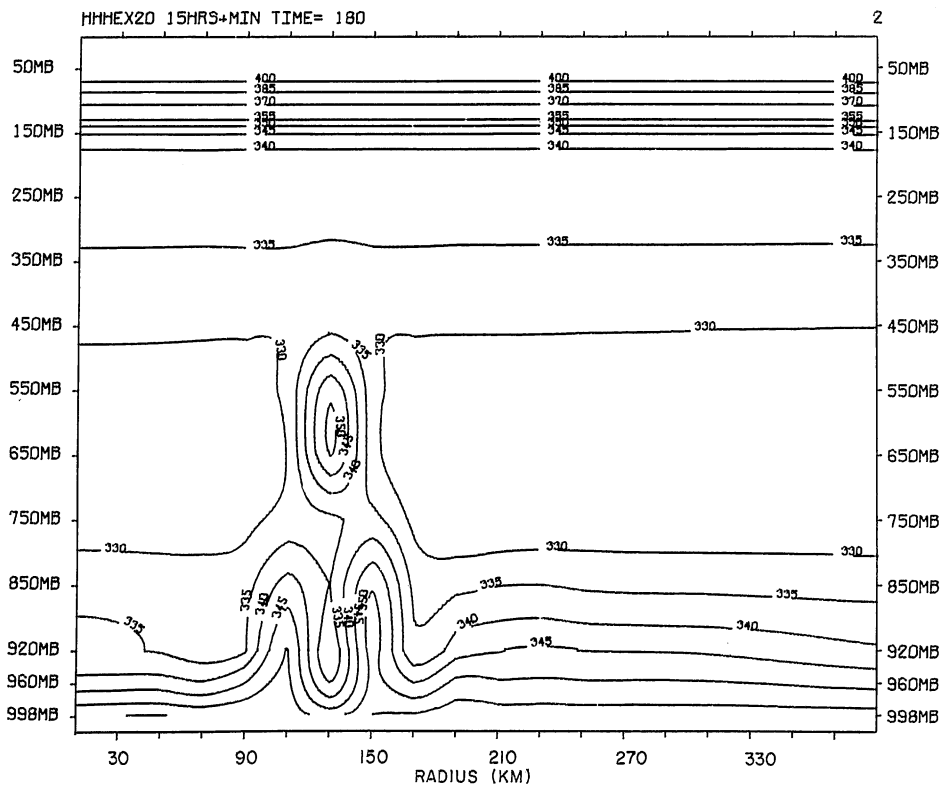

Figure 22.—Vertical cross section of moist static energy at 18:00 h (Exp. 20).

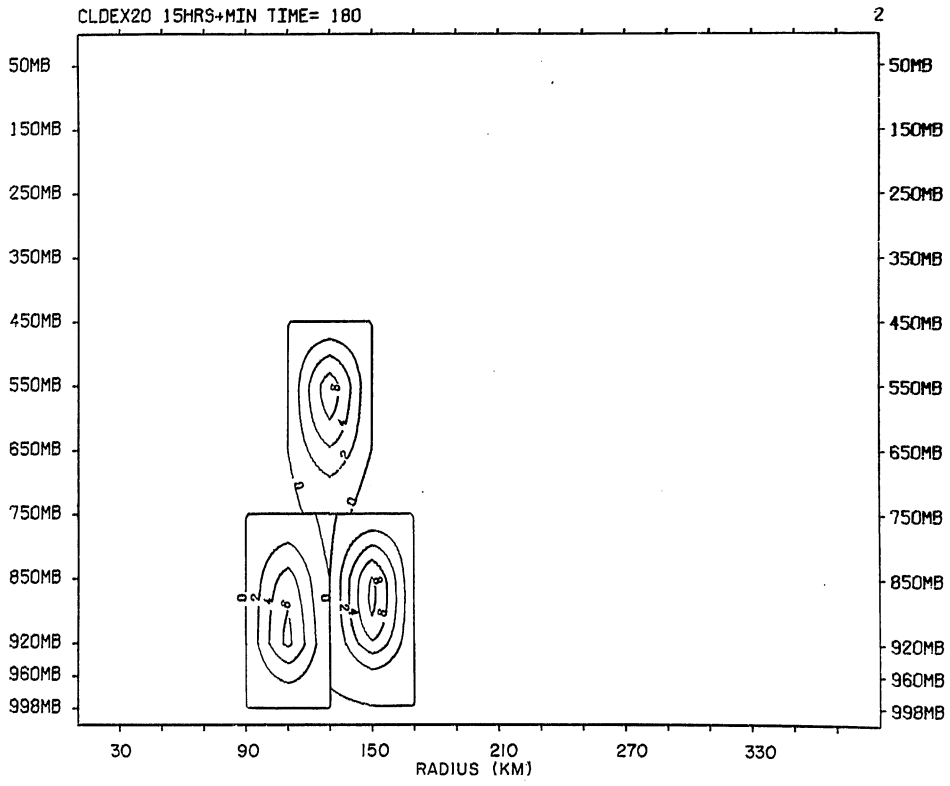

Figure 23.—Vertical cross section of cloud water at 18:00 h (Exp. 20).

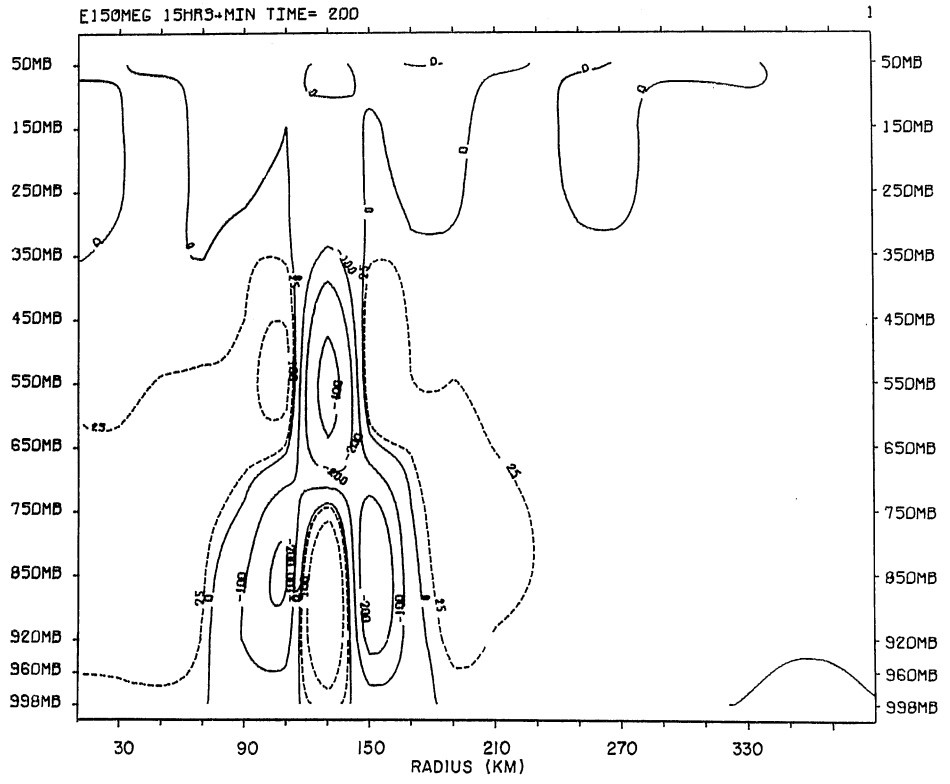

Figure 24.—Vertical cross section of ω at 18:20 h (Exp. 15).

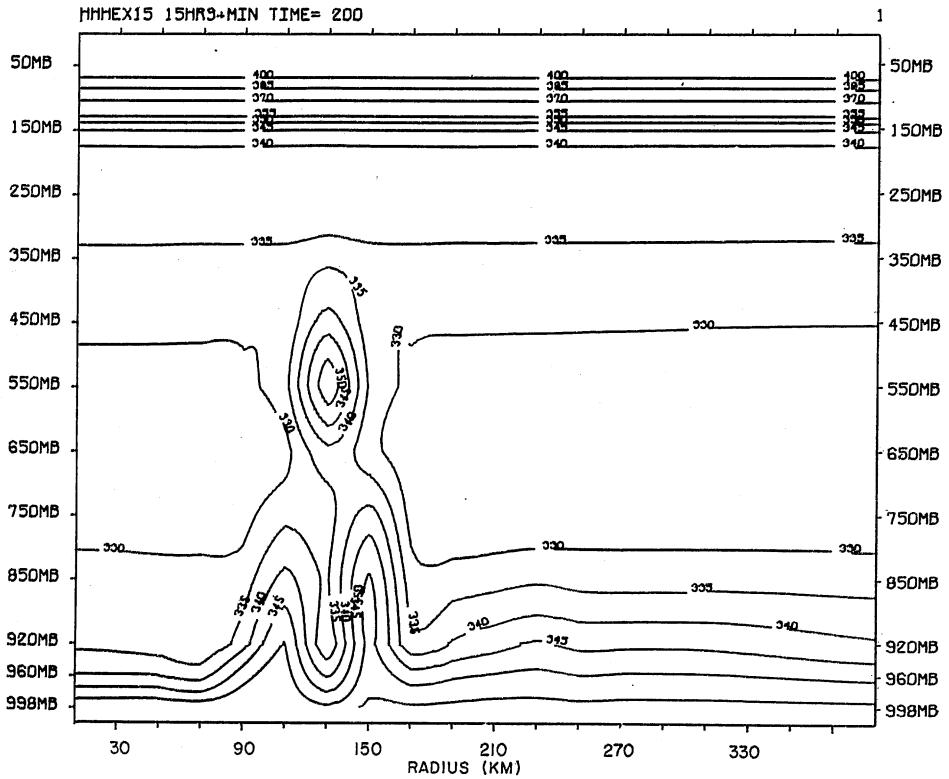

Figure 25.—Vertical cross section of moist static energy at 18:20 h (Exp. 15).

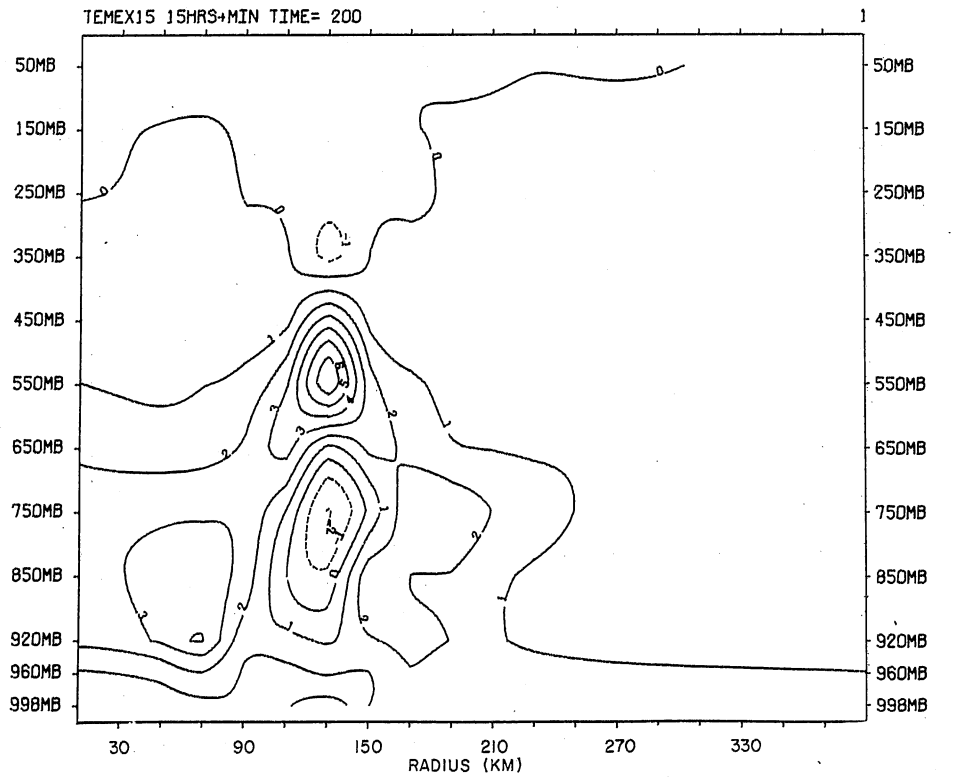

Figure 26.—Vertical cross section of temperature anomaly at 18:20 h (Exp. 15).

structure of the squall system) is not included in most parameterizations, but is clearly of great importance in the real atmosphere.

4.2 Subsequent Developments

By 18:30 h of Exp. 20, the vertical motion maximum associated with C130 (fig. 27) is at 450 mb. The downward motion with D130 has built upward to 650 mb. The cold subcloud air (fig. 28) has spread laterally, and the radial motion field (not shown) indicates that cold air is being carried aloft in the updrafts associated with C150 and C110. The low-level cold air between 80 and 160 km is almost entirely outflow from D130. A strong warm anomaly, splitting the cold air associated with D130, has developed as a result of the unsaturated descent and has worked its way down to the 960-mb level. Zipser (1977) discusses this type of warming in mesoscale downdrafts associated with tropical squall lines. The upper portion of D130 continues to be cold, and the cold air reaches to greater heights. The upward bulge of the low-level isotherms at 150 km results from saturated ascent of absolutely stable air left beneath C150. The vertical growth of cold air at 110 and 150 km indicates the start of the process that will ultimately produce downdrafts below C150 and C110. Indeed, the surface pressure-gradient force (table 2) is already divergent at 150 km. As a result of compensating subsidence, the updrafts on either side of D130 have become broader, and the situation is tending toward new cloud development at 170 and 90 km. Figure 29 shows C090 has already formed.

By 19:00 h significant changes in vertical motion have taken place (fig. 30). The updraft maximum associated with C130 is now between 250 and 350 mb. The low-level updraft at 170 km has intensified, and a well-developed cloud (C170) is now present at that location (fig. 31). The updraft to the rear of D130 has become broader and weaker. D130 now reaches up to 450 mb and has broadened.

Comparisons of the temperature anomaly field (fig. 32) and the vertical motion (fig. 30) show that processes that must lead to still further changes in the vertical motion field are at work. Very dramatic subsidence warming in the lower part of D130 is now apparent, and the surface-pressure field now shows a trough (tables 1 and 2) at that location. The low-level motion at 130-km radius is, therefore, toward convergence. On the other hand, the low-level cold air beneath C150 and C110 has induced surface-pressure ridges in those locations, and low-level divergence is being accelerated beneath the cloud elements there.

The tall, cold column beneath C150 has been created by processes similar to those that produced cold air in the wake of C130, but with important help from cold advection. The cold air at 150 km is convectively stable (fig. 33), except in the 960- to 850-mb layer. Above 850 mb, cooling is produced by saturated stable ascent. Between 960 and 850 mb, the cooling is produced by unsaturated ascent of conditionally unstable air and below 960 mb the ascent has been unsaturated and stable. The pinching of the cold air at 920 mb reflects a region where the updraft at 150 km undergoes strong dynamic entrainment (horizontal advection) of very warm air that has descended in D130. Cloud base for C150 is near 850 mb (fig. 31), and there is precipitation evaporation from there to the surface.

Moist static energy cutoffs have already occurred in C170 and C090. However, these two cloud elements will have altogether different futures. C090 is dynamically entraining air from D130 through its total depth. C170, on the other hand, has, at this time, essentially undilute low-level air from the exterior in its lowest layers. Here, the cutoff has been produced by dynamic entrainment of warm, dry air that descended in the compensating subsidence at 190 km. In contrast to C150, and subsequent cutoffs on the outer flank of the convective system, the low-level cold air plays no direct role in the cutoff of C170.

At 19:30 h, D150 (fig. 34) is well developed. However, thermal changes (fig. 35) that will produce another outward jump of the system are already in progress. D150 is already quite warm and dry (fig. 36) at low levels. On the basis of Zipser's (1977) study, the low humidity values (less than 60%) are not unreasonable. C170 is now centered between 650 and 750 mb (figs. 37 and 38), and cold air has begun to form at low levels in the wake of the stable air beneath this cloud element. At the very lowest levels of the 170-km column, there is cold advection from the interior. In fact, the lowest 100 mb of the 170-km column are being fed by air from D150. We can, therefore, expect the base of C170 to rise and thus make conditions at 170 km still more favorable for cooling the lower part of that column.

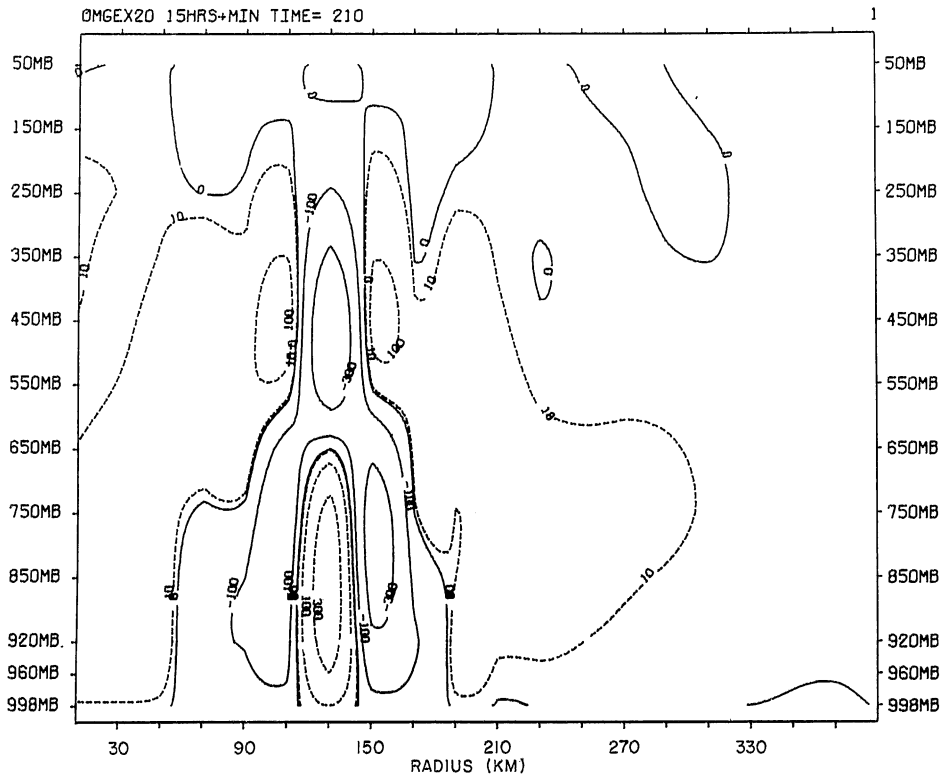

Figure 27.—Vertical cross section of ω at 18:30 h (Exp. 20).

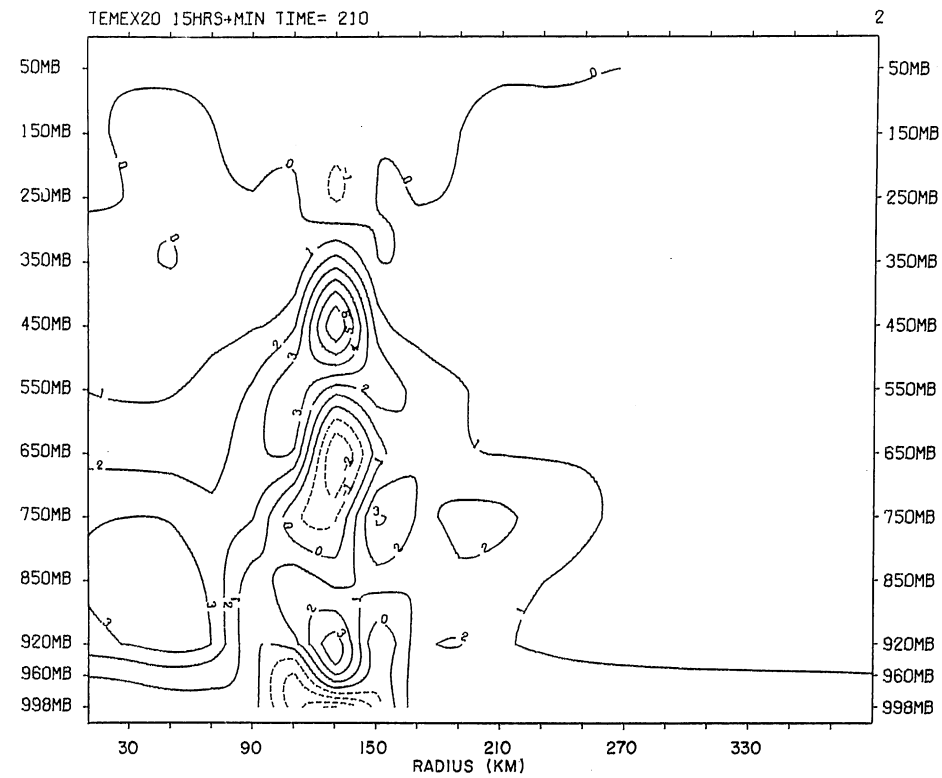

Figure 28.—Vertical cross section of temperature anomaly at 18:30 h (Exp. 20).

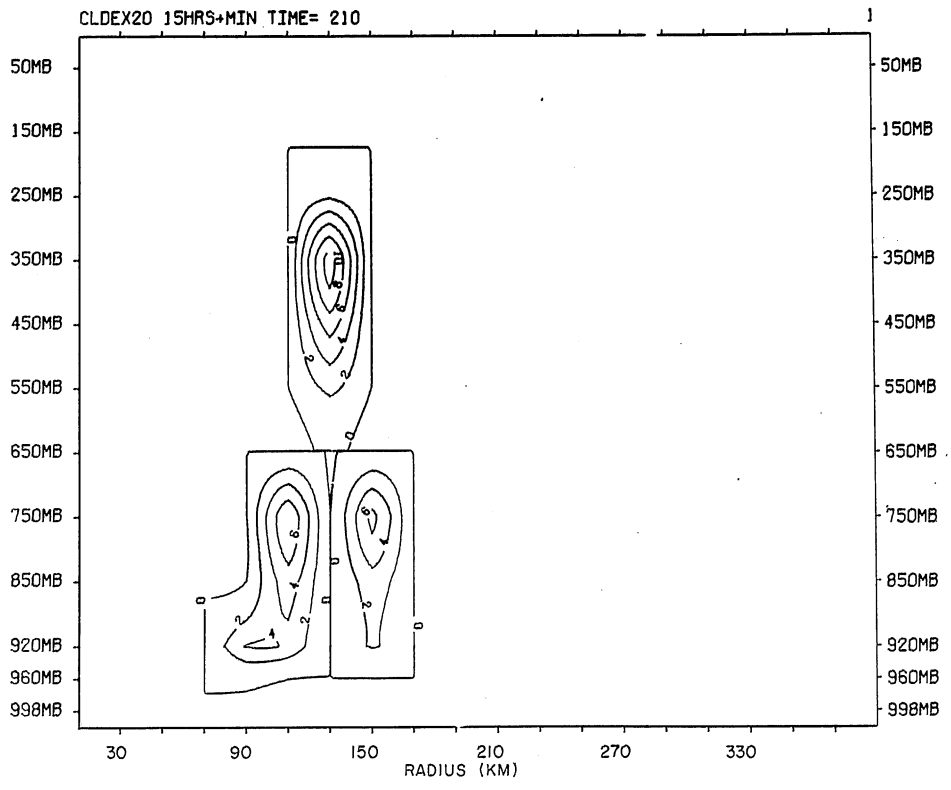

Figure 29.—Vertical cross section of cloud water at 18:30 h (Exp. 20).

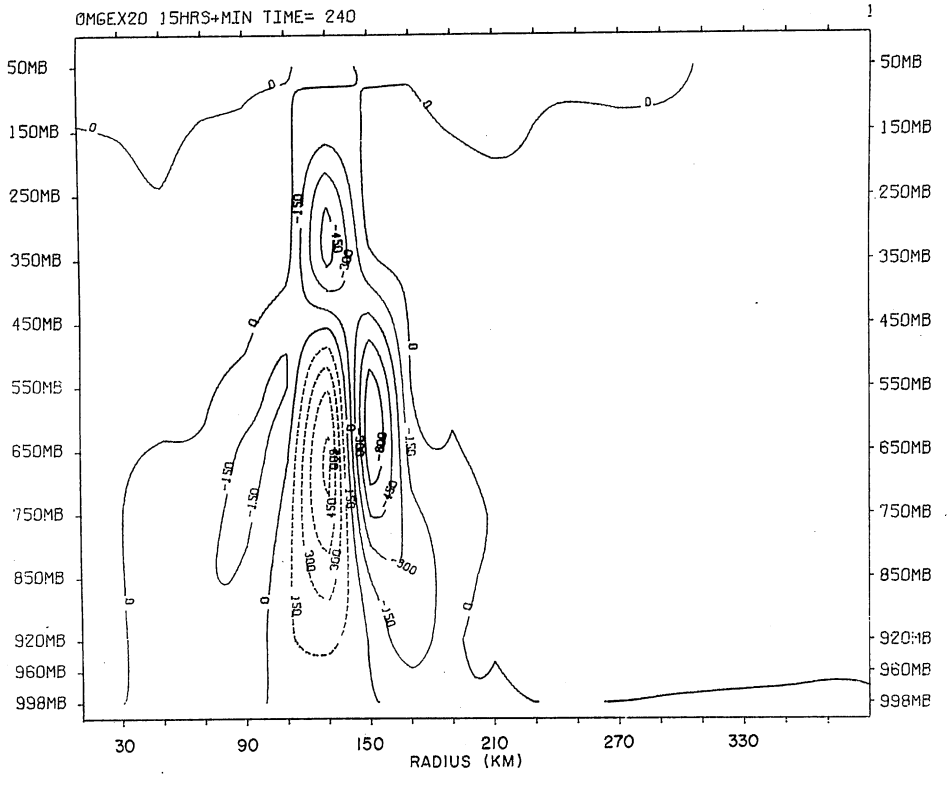

Figure 30.—Vertical cross section of ω at 19:00 h (Exp. 20).

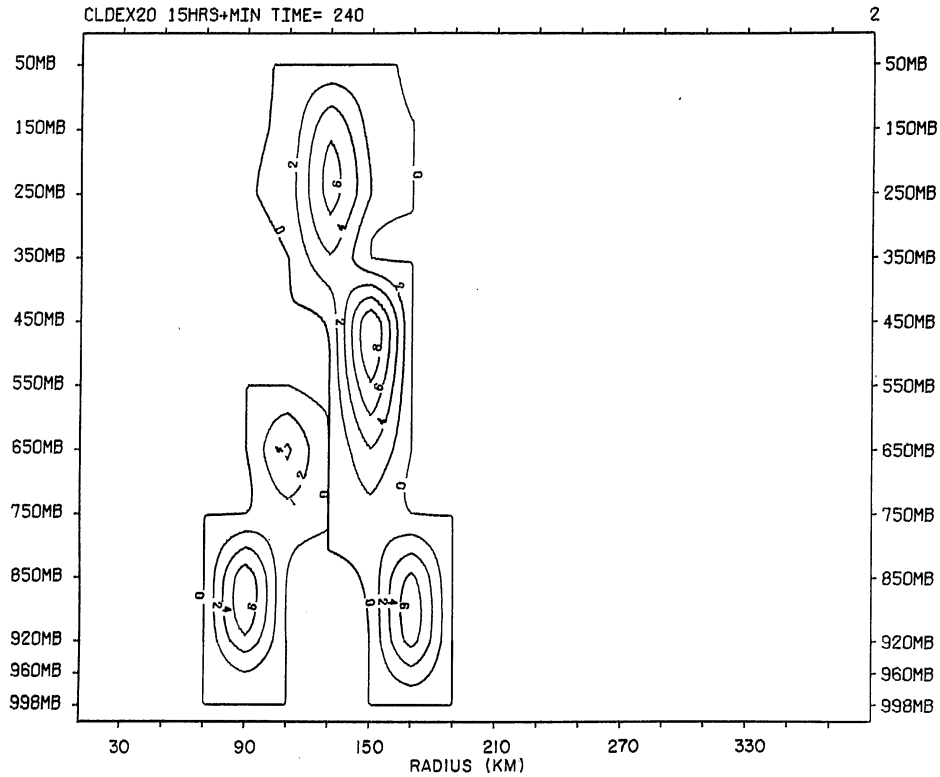

Figure 31.—Vertical cross section of cloud water at 19:00 h (Exp. 20).

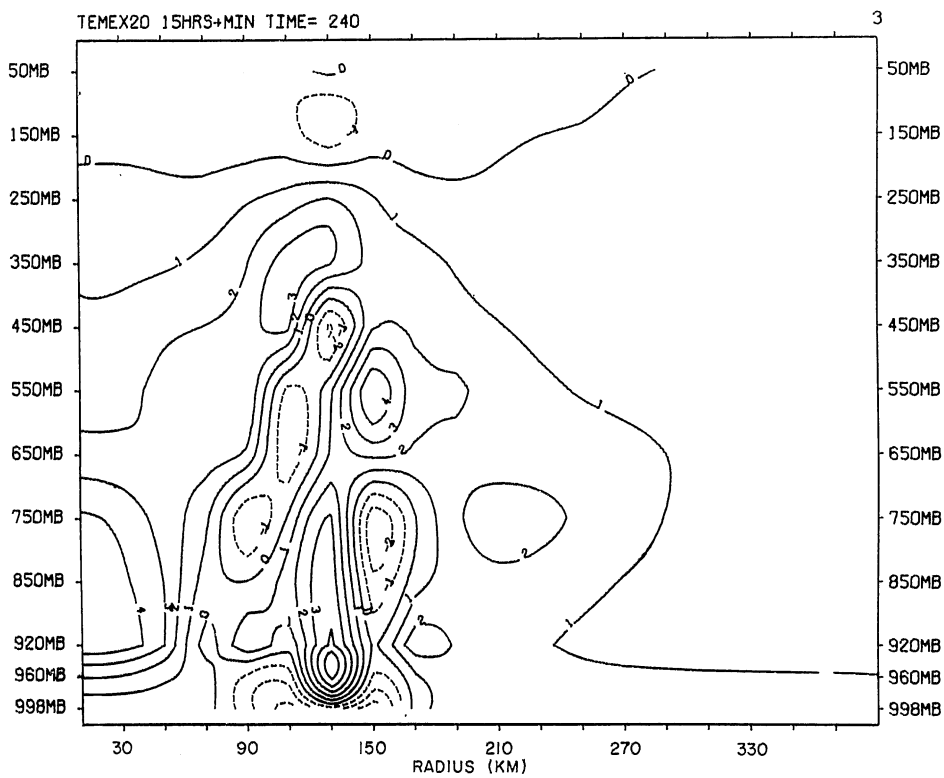

Figure 32.—Vertical cross section of temperature anomaly at 19:00 h (Exp. 20).

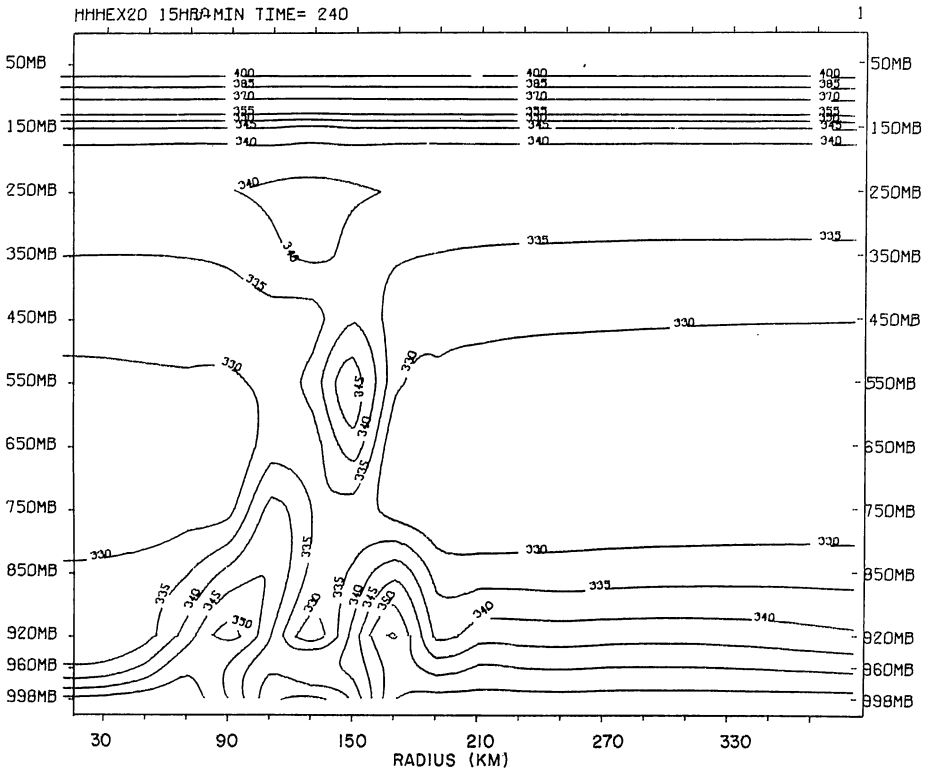

Figure 33.—Vertical cross section of moist static energy at 19:00 h (Exp. 20).

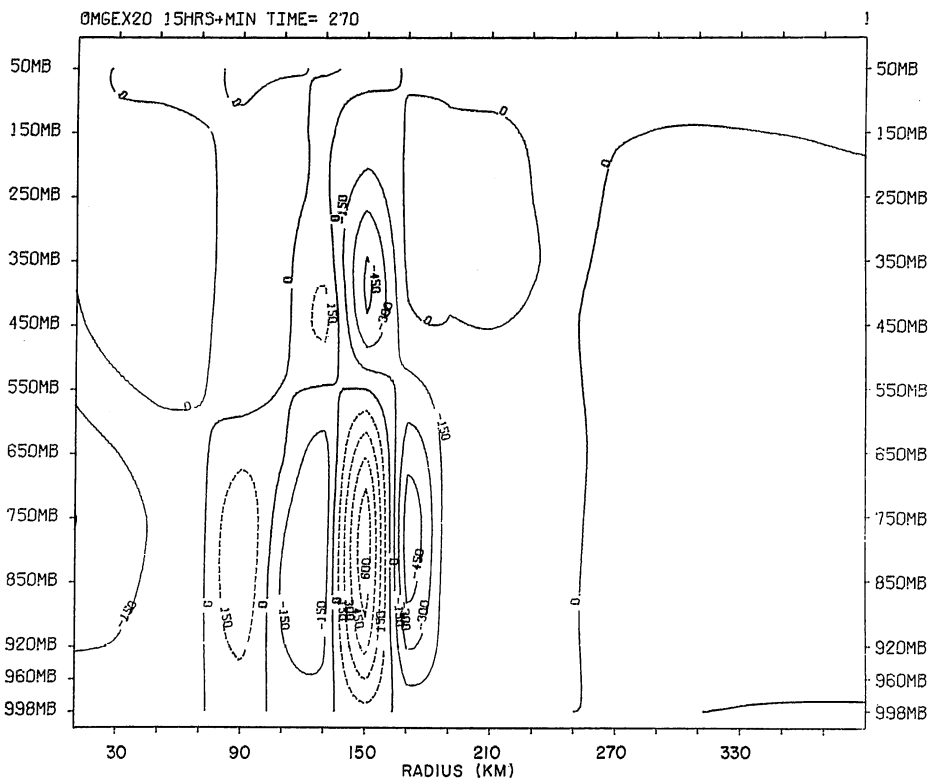

Figure 34.—Vertical cross section of ω at 19:30 h (Exp. 20).

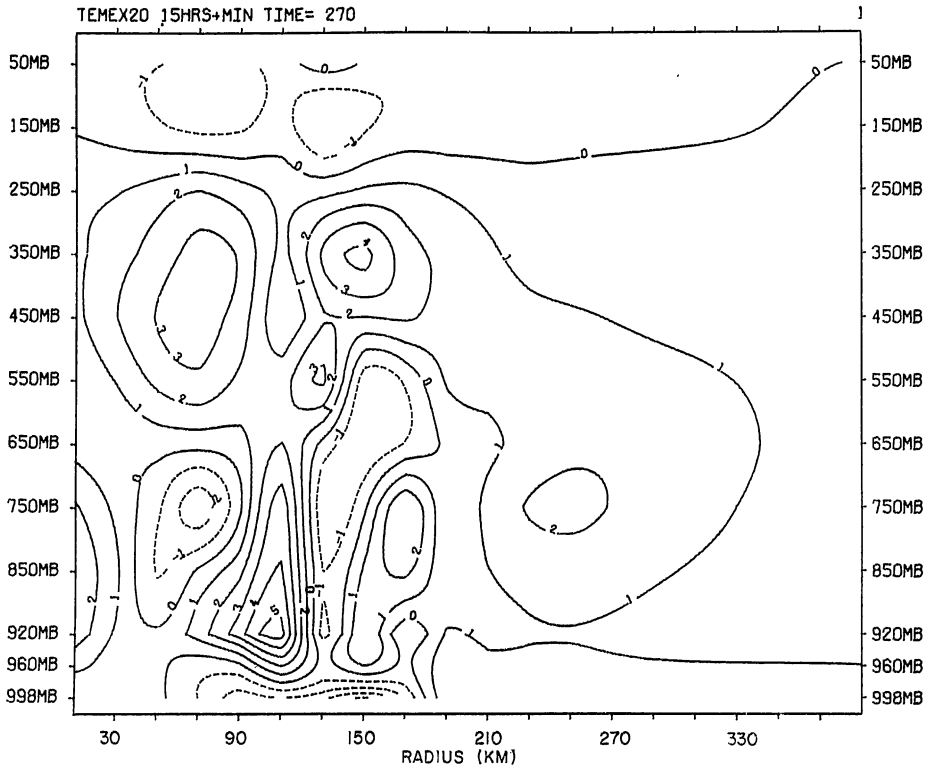

Figure 35.—Vertical cross section of temperature anomaly at 19:30 h (Exp. 20).

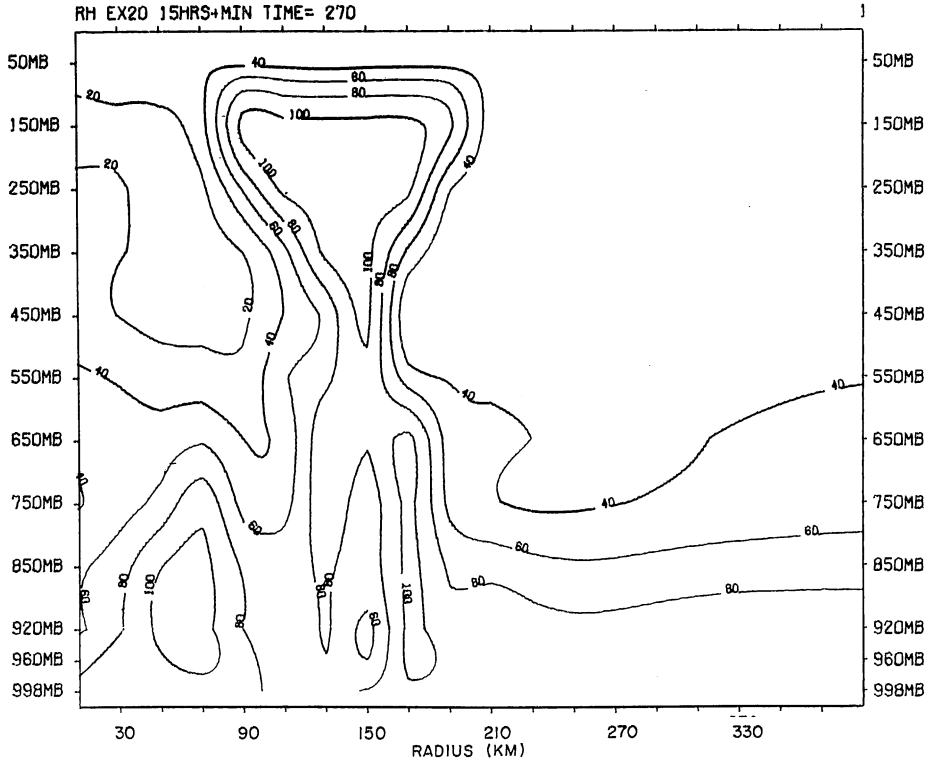

Figure 36.—Vertical cross section of relative humidity at 19:30 h (Exp. 20).

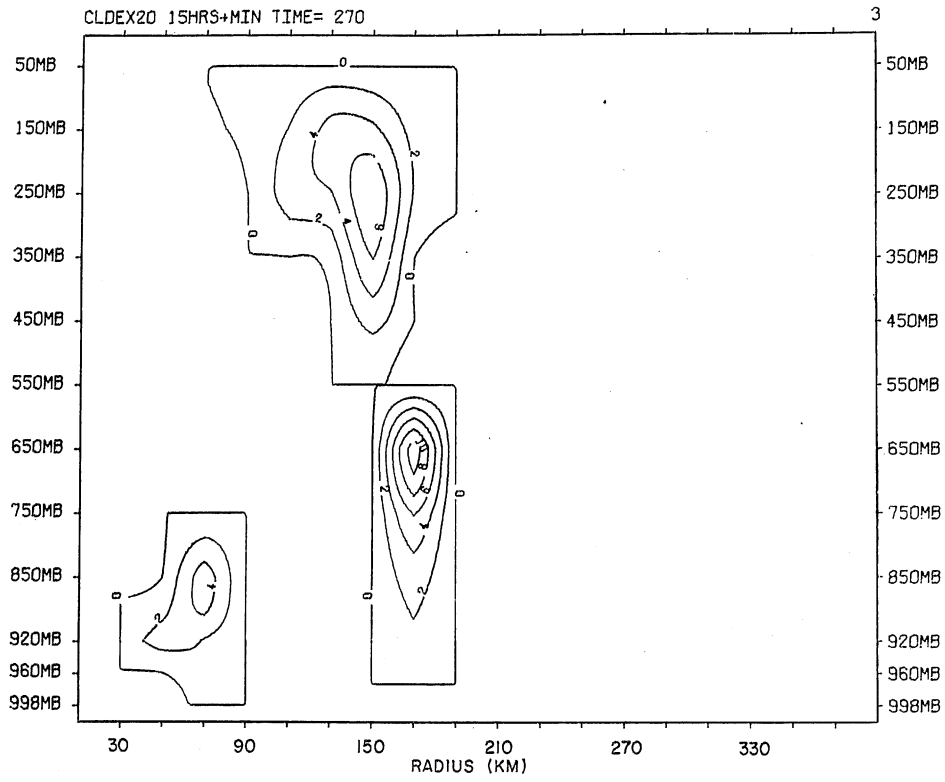

Figure 37.—Vertical cross section of cloud water at 19:30 h (Exp. 20).

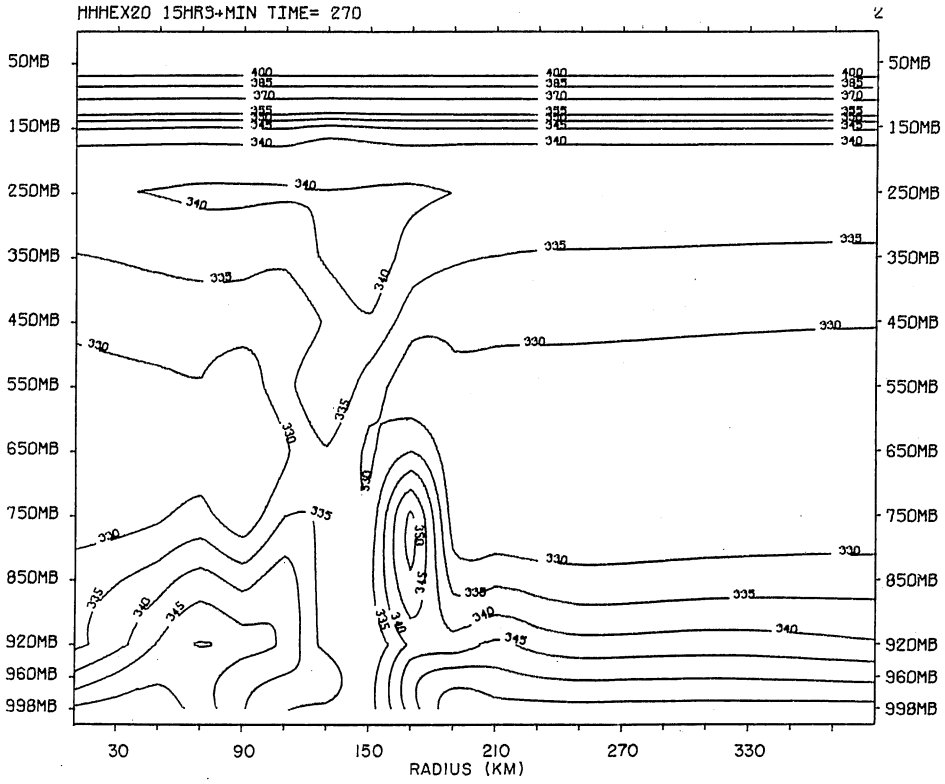

Figure 38.—Vertical cross section of moist static energy at 19:30 h (Exp. 20).

The very warm air at 110 km (fig. 35) is a result of dry subsidence that occurred there between 19:00 and 19:30 h. The broad area of ascent ahead of C170 (fig. 34) is associated with a gravity wave of the second internal mode that moves radially outward at about 22 m s^{-1}. The rainwater pattern (fig. 39) shows precipitation reaching the ground from C150 and C170 and, to a lesser extent, from older cloud elements that are now eroding in the upper troposphere.

The important physical mechanisms involved in the propagation and maintenance of the convective system have been illustrated by the description given above. Although subsequent clouds and cold downdrafts do not have identical histories, there is sufficient correspondence to warrant the less detailed account of them that follows.

By 20:30 h another jump of the system has been completed (figs. 40 and 41), and D170 and C190 are well established. The bottom of the updraft associated with C190 has already started to broaden as a result of compensating subsidence near 210 km (table 2). By 21:30 h (figs. 42 and 43), D190 and C210 have developed. The broad updraft, located radially outward from C210, is associated with a second internal gravity wave that has been excited by the convection. The lowest portion of the updraft at 210 km contains cold air (not shown) that has been advected there by the circulation associated with D190. The moist static energy cutoff (fig. 43) associated with C210 is almost entirely a result of the influx, at low levels, of this cold air, rather than a result of compensating subsidence as in the earlier cases. Because of the interference pattern set up by the gravity wave, compensating subsidence does not occur close to C210. C230 forms in the broad regions of ascent associated with the gravity wave. (C190 formed in a somewhat similar fashion.) The development of C230 is strongly aided by the spreading of cold air at low levels by the circulation associated with D190. By 22:10 h (not shown), cold air from D190 underruns C230 and reaches even farther radially outward.

By 22:40 h (figs. 44 and 45), C230 and D210 are formed. The updraft with C230 is substantially weaker than in previous cases. The moist static energy cutoff (fig. 45) with C230 is complete and, again, the cutoff mechanism has been cold air advection from the downdraft to the rear. This is particularly evident in the moist static energy, which shows a different structure beneath C230 than was the case for the earlier cutoffs, such as C130 and C150. In those cases, a thin layer of exterior boundary-layer air was present close to the surface below the cloud element. Here we see that this is not the case. The multicell structure of the system is clearly delineated by the cloud water (fig. 46). Four elements are visible here, and there is a close resemblance to the structure of the multicell hail storm discussed by Browning et al. (1976), (fig. 3).

The above description is based on inspection of the data at 5-min intervals between 15:00 and 24:00 h. The system was followed with hourly data until 78:00 h. Through 78:00 h, successive cutoffs of moist static energy occur at larger and larger radii. The convective system is also evident in the precipitation and vertical motion data. Beyond 78:00 h, there is no further evidence of the system. Between 24:00 and 40:00 h, before the convection moves out of the uniform 20-km domain, the system is generally quite weak in comparison with the data shown above. However, a flare-up at about 36:00 h (when the forward cloud elements are located near 350 km) brings the system temporarily to its earlier intensity. The system is near 520-km radius when it can last be detected at 78:00 h. Its demise is probably partly due to physical causes and partly due to numerical causes. Horizontal resolution, at 529-km radius, has expanded to 30 km and, also, by this time, the hurricane circulation (figs. 3 and 4) is well developed, thus placing the squall system in a broad region of compensating subsidence associated with the eyewall.

Figure 47 shows, as a function of the radius at which each cloud between 15:00 and 24:00 h formed, the largest vertical motion associated with the element in its lifetime and the pressure level at which that maximum vertical motion occurred. After C150 successive clouds have smaller maximum vertical motion, and these maxima occur at lower and lower levels. Table 3 shows for each radius the time that various significant events took place. Cold advection at low levels from the downdraft to the rear begins closer to the time of cloud development with each new cloud. Indeed, at 250 km, cold advection actually starts before the cloud forms. Thus, the contribution of the cold air from the rear to a hydrostatic pressure rise at low levels appears to explain the diminishing intensity of vertical motion with successive cloud elements during this period.

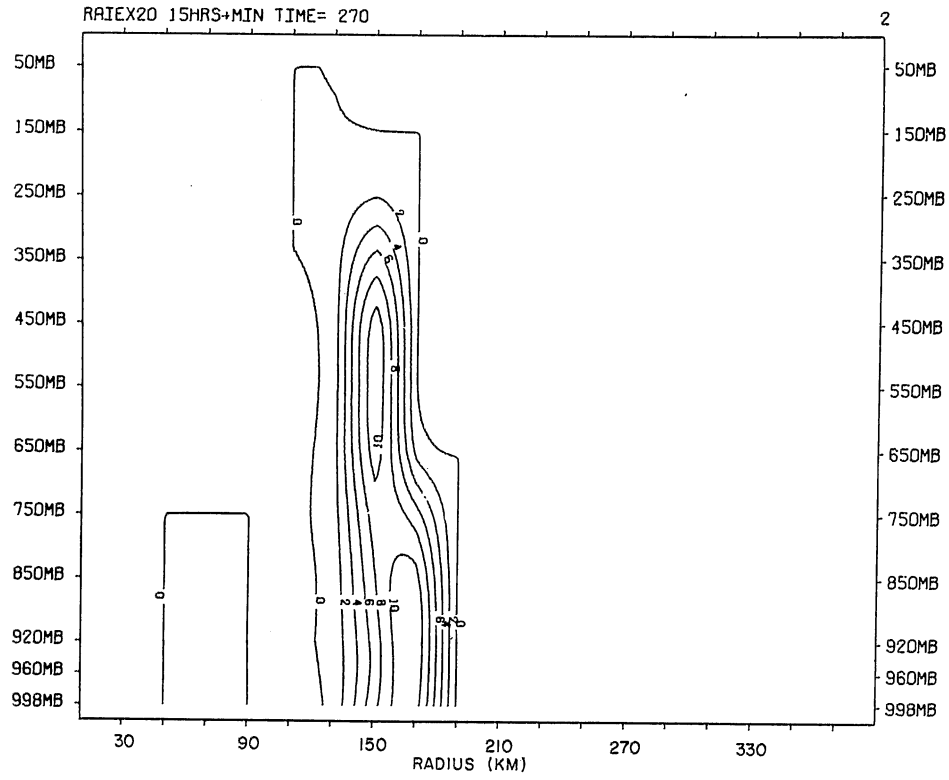

Figure 39.—Vertical cross section of rainwater at 19:30 h (Exp. 20).

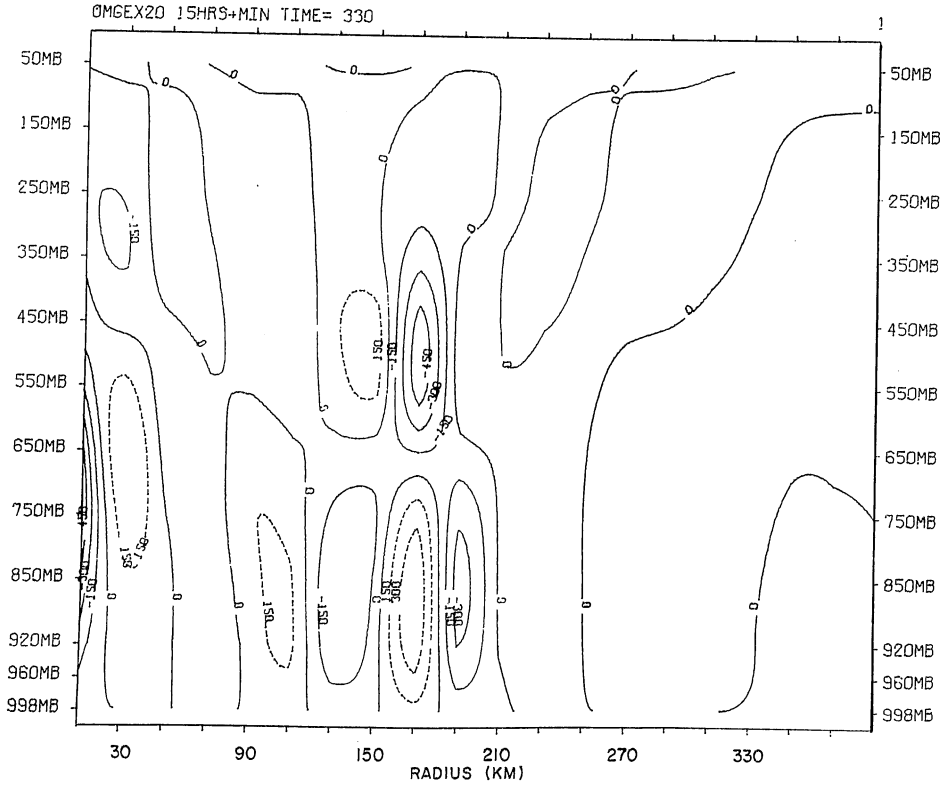

Figure 40.—Vertical cross section of ω at 20:30 h (Exp. 20).

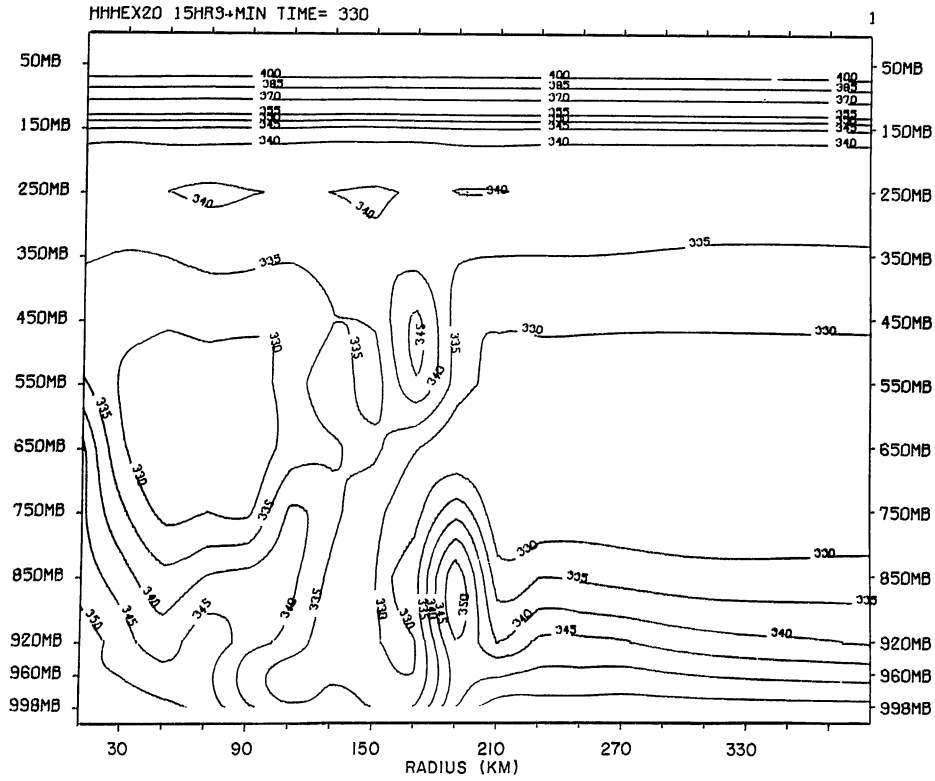

Figure 41.—Vertical cross section of moist static energy at 20:30 h (Exp. 20).

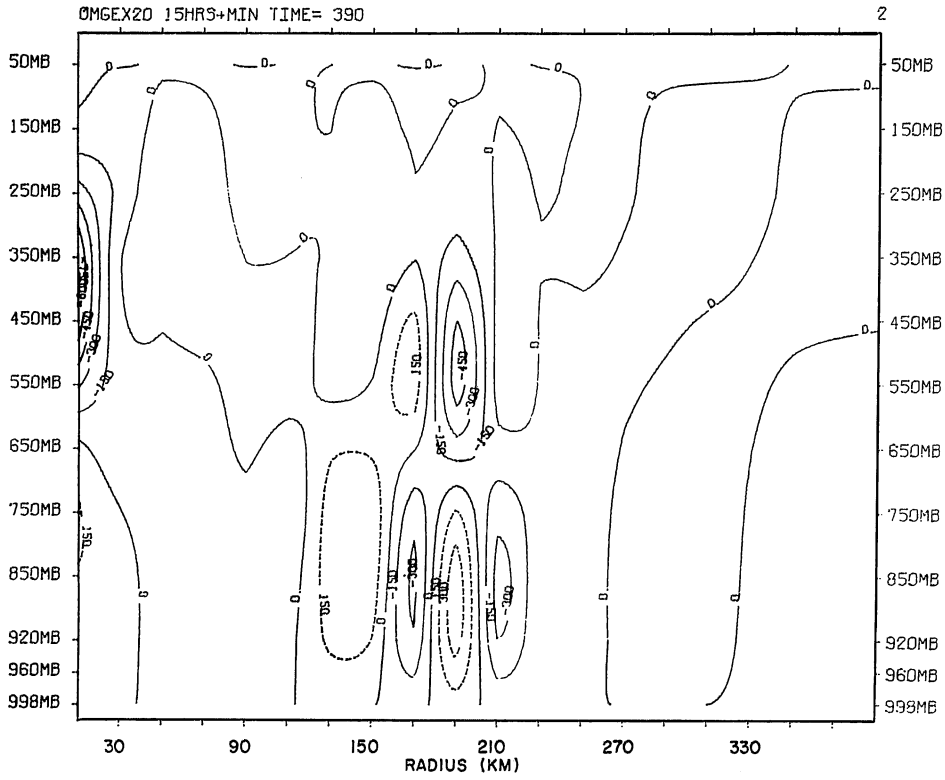

Figure 42.—Vertical cross section of ω at 21:30 h (Exp. 20).

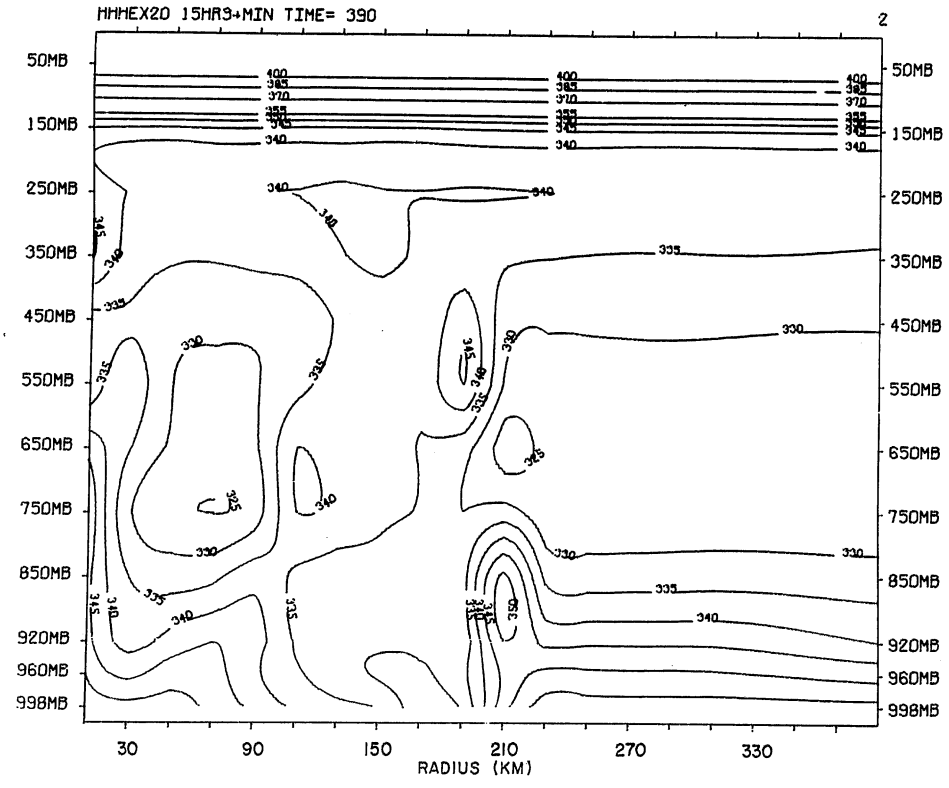

Figure 43.—Vertical cross section of moist static energy at 21:30 h (Exp. 20).

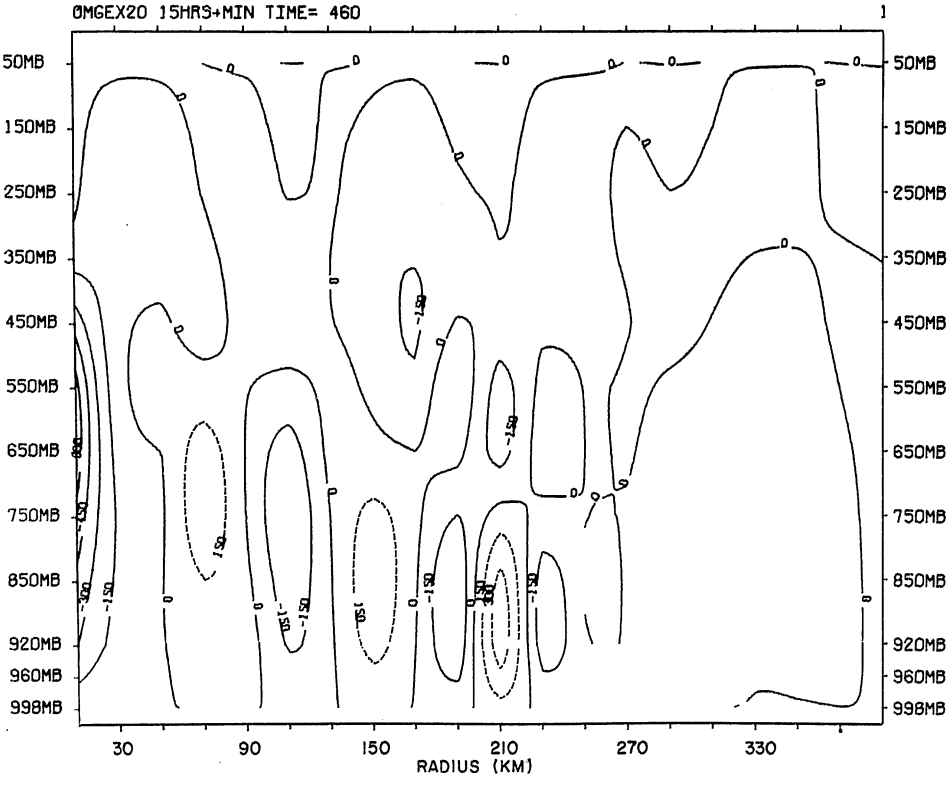

Figure 44.—Vertical cross section of ω at 22:40 h (Exp. 20).

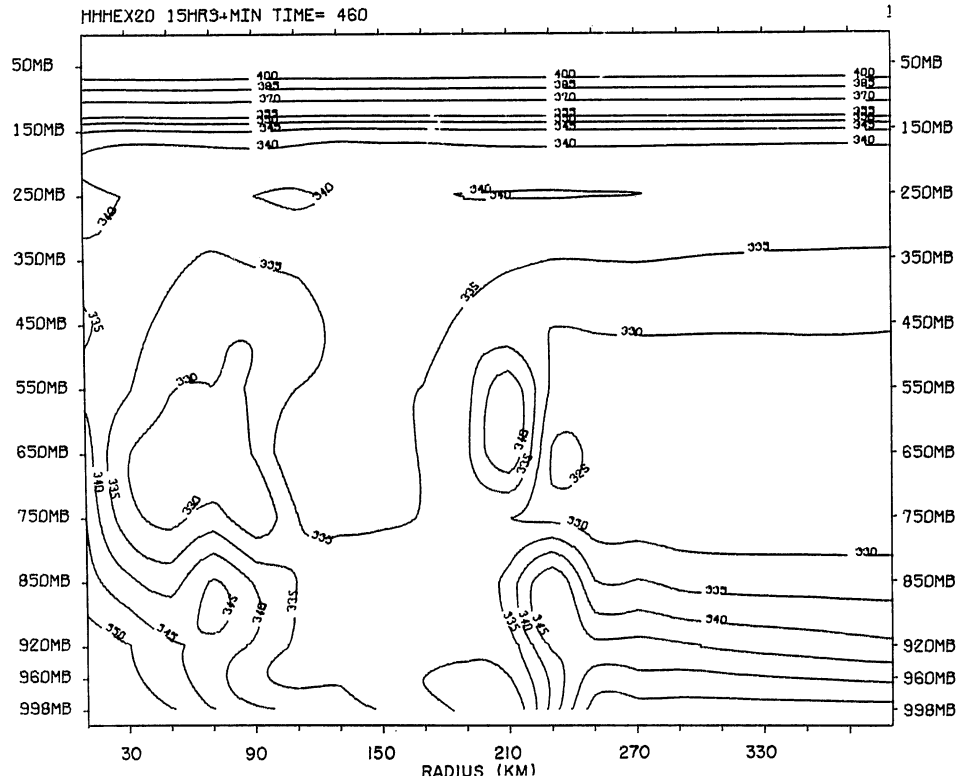

Figure 45.—Vertical cross section of moist static energy at 22:40 h (Exp. 20).

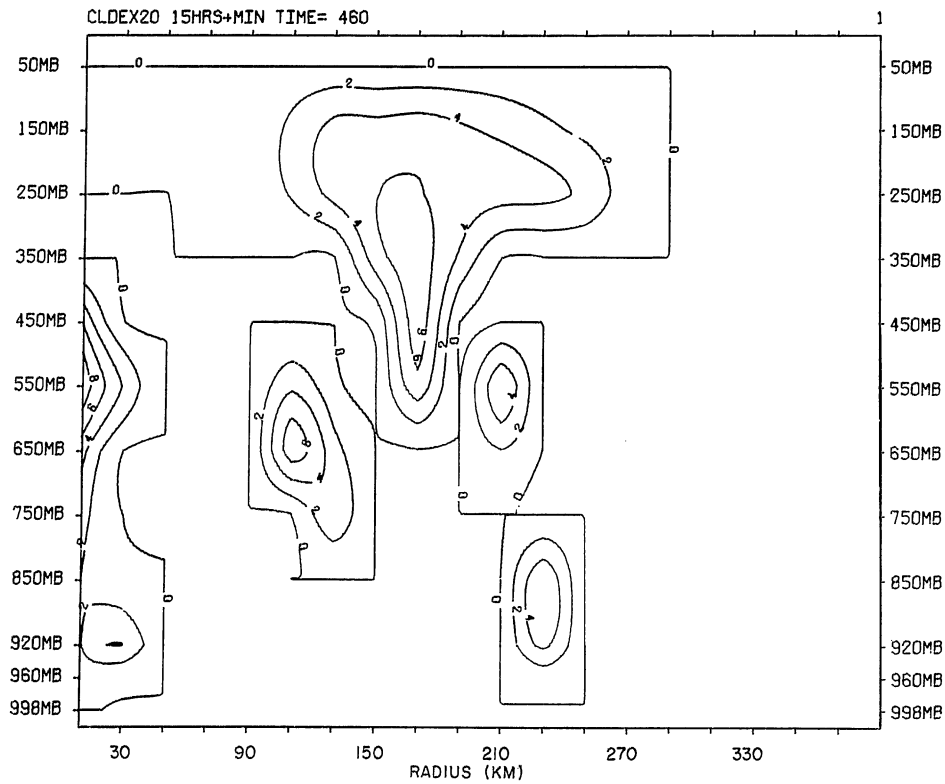

Figure 46.—Vertical cross section of cloud water at 22:40 h (Exp. 20).

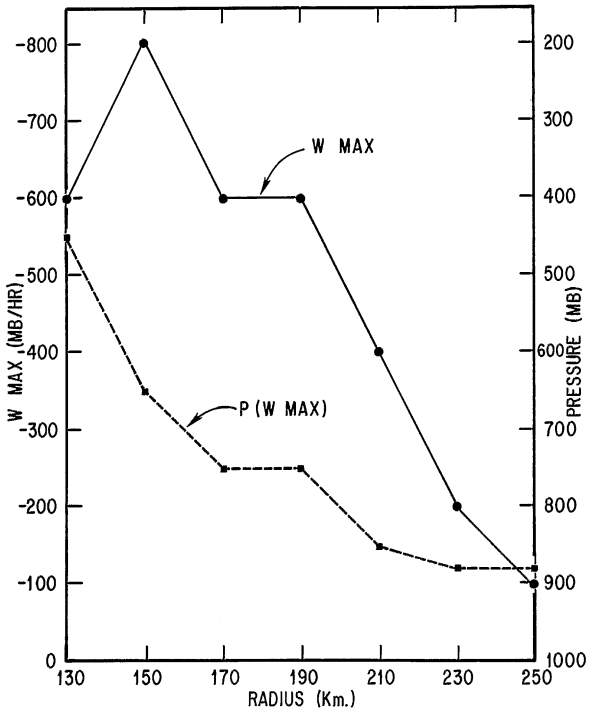

Figure 47.—Data from Exp. 20. Abscissa is the radius at which clouds formed between 10:00 h and 24:00 h. Left ordinate is maximum vertical motion $\omega(=dp/dt)$ that occurred in that cloud during its lifetime (solid curve). The right ordinate is the height (base-state pressure) at which that maximum vertical motion occurred (dashed curve).

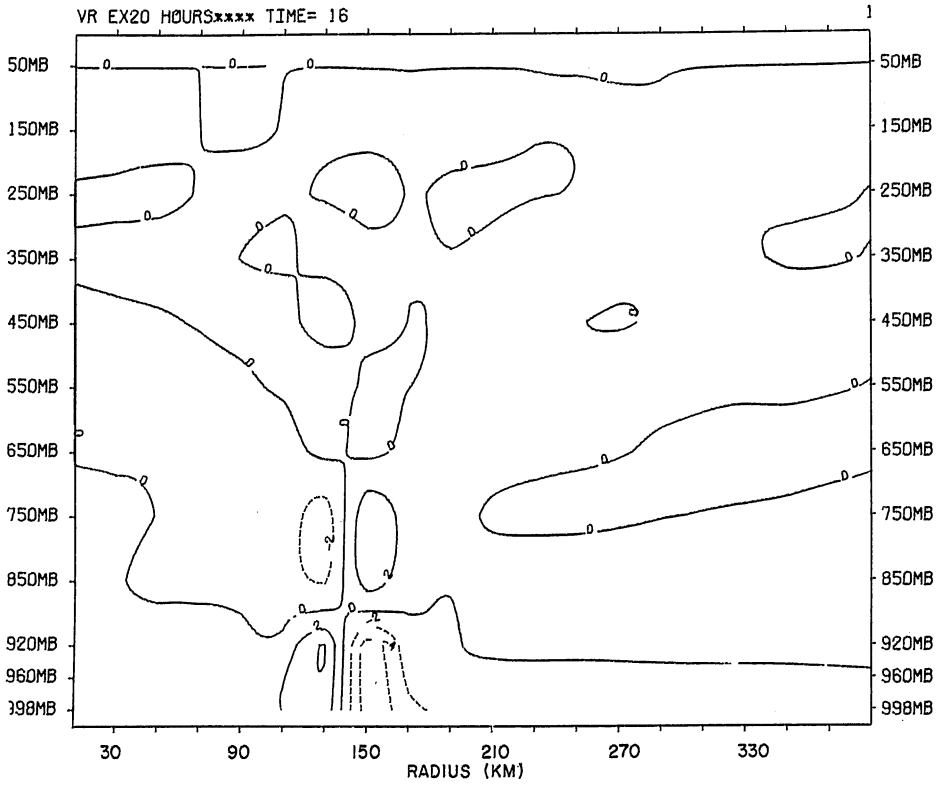

Figure 48.—Vertical cross section of radial component of the wind at 16:00 h (Exp. 20). Isotachs are at intervals of 2 m s^{-1}. Negative values (inflow) are dashed.

Table 3. Times from 15:00 h to 24:00 h at which significant events from cloud formation to downdraft formation occur at each radius between 130 and 250 km*

Radius (km)	Event						
	Cloud forms	Rain reaches surface	Cold advection starts in the boundary layer	Cutoff of moist static energy occurs energy occurs	Spatial rain max. reaches grid point	Surface pressure-gradient force becomes divergent	Downdraft forms
130				16:15		16:25	17:15
150	17:25	17:35	18:00	18:05	18:25	18:45	18:55
170	18:35	18:50	19:05	18:55	19:30	19:40	19:50
190	19:55	20:00	20:00	20:10	20:25	20:55	21:10
210	20:50	21:05	21:05	21:05	21:45	21:50	22:10
230	21:50	22:05	21:55	22:05	22:50	22:50	23:15
250	22:50	23:25	22:45	23:15	>24:00	23:50	>24:00

*Table was constructed by study of time-height cross sections of 5-min history data at each radius, as well as the study of radial profiles at 5-min intervals.

Table 3 also shows that at each radius the time between cloud formation and downdraft formation ranges from 75 to 90 min. Clouds C120 through C250 form at hourly intervals (as detected from data at 5-min intervals), thus giving the system an apparent progression of 20 km h^{-1}. One should also note that the later cloud developments are closely correlated with the development of a divergent surface pressure-gradient force at the next interior grid point, whereas the earlier cloud developments are poorly correlated. Mechanical lifting by cold subcloud air becomes more important in the later cloud developments. It is of less importance for earlier ones, where compensating subsidence plays the dominant role in the generation of convergent surface-pressure forces that produce the lifting needed for cloud formation. Table 4 shows the accumulated precipitation as a function of time and radius.

Figures 48, 49 and 50 show the radial wind component at 16:00, 19:00, and 22:00 h. The increasing depth of the inflow layer (as shown by the rise of the zero line) as the mesoscale convection develops is striking. At 22:00 h, the inflow layer reaches to about 400 mb (fig. 50) and is capped by a thin layer of strong outflow, much as has been observed in some studies of tropical cloud clusters and weak tropical waves (e.g., Williams and Gray, 1973). This vertical structure, as simulated here, appears to be a natural consequence of the dynamic and thermodynamic processes that control the convection and, apparently, does not require radiative effects for its existence.

5. DISCUSSION

The simulation of so many of the structural features and physical processes of tropical mesoscale systems by this crude model is rather remarkable. However, the value of this model cannot be primarily as a vehicle for the study of moist convection since the model is obviously limited for that purpose. Rather, as discussed by Rosenthal (1978), the results of this calculation provide a possible alternative to the traditional schemes of parameterizing

Table 4. Accumulated precipitation (mm) as a function of time and radius (Exp. 20)

Time (h:min)	Radius (km)							
	110	130	150	170	190	210	230	250
15:00		T						
16:00		2.0						
17:00		7.0						
18:00	0.2	16.9	0.2					
19:00	4.2	24.3	13.0	T				
20:00	4.6	24.9	26.9	17.4	T			
21:00	5.9	25.2	26.9	28.6	8.6			
22:00	10.2	25.5	27.0	29.2	26.2	6.9		
23:00	10.8	25.9	27.2	29.3	26.7	17.7	2.7	
24:00	11.5	25.9	27.3	29.7	26.7	18.8	5.8	0.4

Note: T indicates a trace of <0.1 mm.

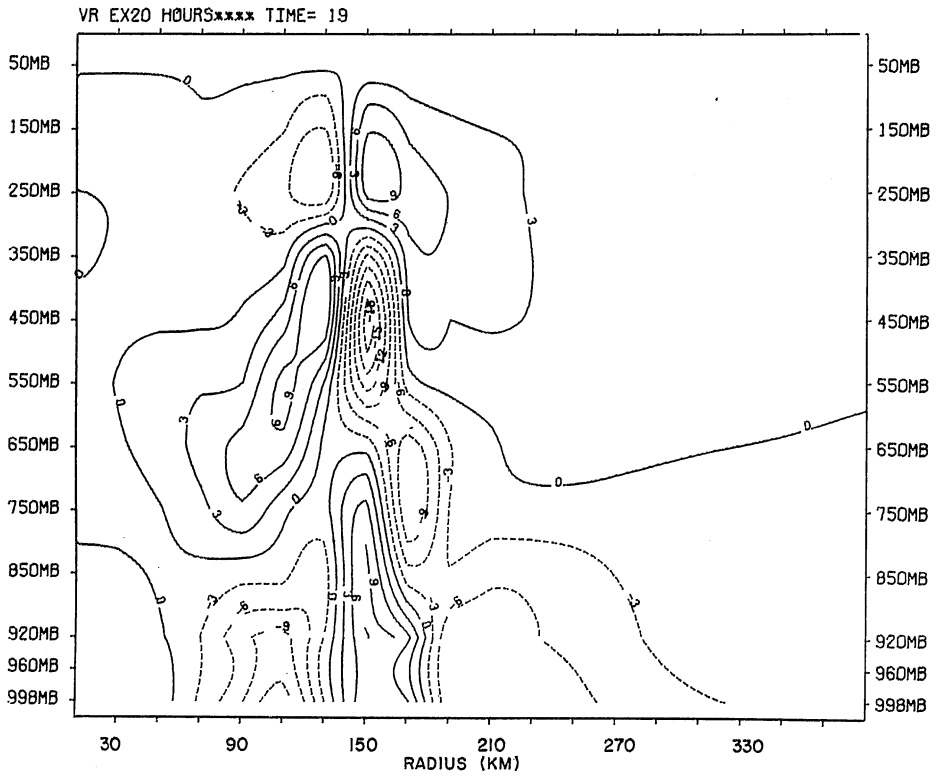

Figure 49.—Vertical cross section of radial wind component at 19:00 h (Exp. 20). Contour interval is 2 m s^{-1}.

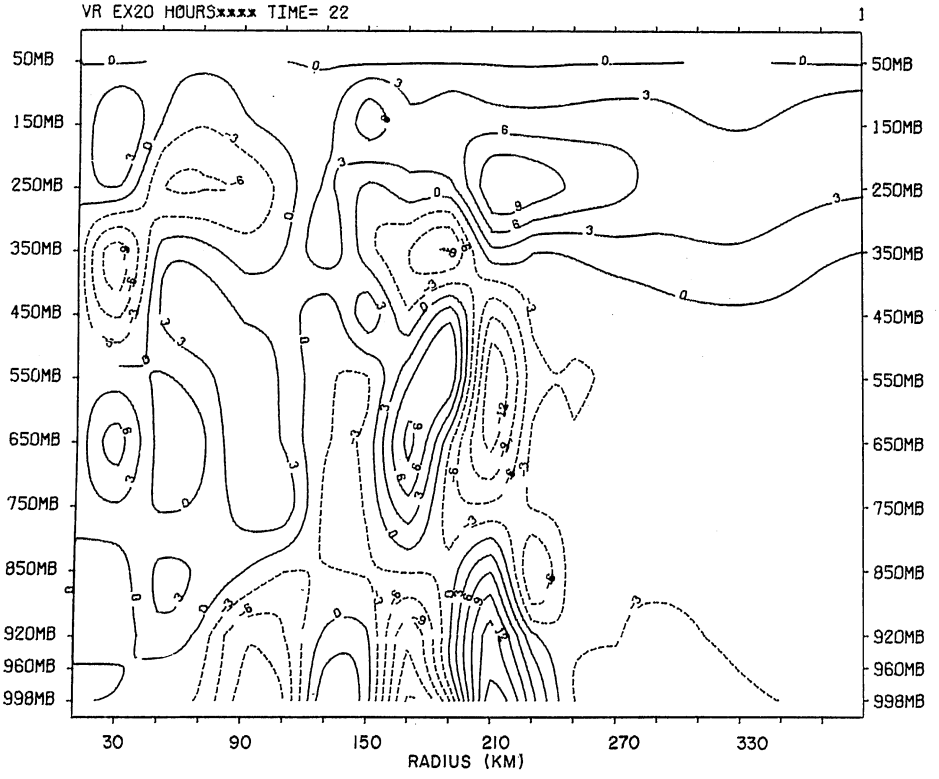

Figure 50.—Vertical cross section of radial wind component at 22:00 h (Exp. 20). Contour interval is 3 m s^{-1}.

cumulus clouds in numerical models with horizontal resolutions of a few tens of kilometers.[1] In Rosenthal (1978), we were able to show that the explicit calculation simulates the characteristic structural features of the mature hurricane. We have now shown that the explicit calculation crudely, but with a fair degree of reality, simulates the multicell propagating squall lines observed in the tropics.

To our knowledge, the cloud-subcloud layer interactions that occur in the presence of deep, precipitating cumulus, and that have recently been described (e.g., Zipser, 1969; Miller and Betts, 1977; Betts, 1976; Seguin and Garstang, 1976), have not, as yet, been realistically parameterized (in a prognostic sense). Yet these interactions, or at least very similar ones, are simulated as a natural consequence of the moist convection in the explicit calculation. Of primary interest is the stabilization of the low troposphere, particularly the subcloud layer, that is observed to occur in the wake of these systems. In the real atmosphere, this stabilization is a result of precipitation evaporation, convective-scale (cold and saturated) downdrafts, and mesoscale (warm and unsaturated) downdrafts (Zipser, 1969, 1977; Betts, 1976; Miller and Betts, 1977). The studies of Houze (1976, 1977), Zipser (1969, 1977), and Seguin and Garstang (1976), as well as others, show that in comparison with the horizontal scales of interest here, this stabilization occurs over large horizontal areas (50 to 100 km) to the rear of the main moist updrafts. Zipser (1969) emphasizes the importance of this stabilization in preventing the development of new moist convection until air-sea exchange processes can restore the low levels to a condition resembling the undisturbed base state. Fritsch (1975) suggested that the processes that stabilize the low troposphere may represent the most important modes of interaction through which moist convection stabilizes its environment.

Although this model does not simulate the cold, saturated, convective-scale downdraft, the downdrafts that are simulated, together with precipitation evaporation, do provide the observed type of stabilization (Zipser, 1969, 1977) as the data at 19:00 h (figs. 32 and 33) demonstrate. The moist static energy (fig. 33) between 110- and 150-km radii very closely resembles Zipser's (1969) (fig. 8) time cross section of equivalent potential temperature after the passage of a squall line during the Line Islands experiment. The temperature anomalies (fig. 32) show evidence of the shallow cold pool at low levels discussed by Zipser (1977) and Betts (1976). This feature is of major importance (both in the real atmosphere and in the simulation) in the organization and maintenance of the moist convection. In agreement with the observations of many investigators, the stable region to the rear of the surface position of the main updraft is a region of heavy precipitation. This is verified by the data of 19:30 h (figs. 34, 38, and 39).

The key to a meaningful definition of CISK, as emphasized in the original paper by Charney and Eliassen (1964), is the *cooperative interaction* of the convective cells and the larger scale. The latter organizes the convection and, through low-level convergence, supplies the warm, moist air that fuels the convective cells. The *ensemble* of convective clouds, in turn, through the release of latent heat, provides a heat source that allows the larger-scale system to grow.

Observational studies of cumulus convection over the tropical oceans, however, have indicated that not all moist convection is cooperative in the sense just described. In certain situations, weak synoptic-scale systems trigger cumulus convection that takes on a squall-line mesoscale organization and then overwhelms the synoptic scale (Zipser, 1977; Frank, 1977; Lilly, 1975). When this occurs, the synoptic scale appears to exert little or no influence on the moist convection. Despite the organization of the cumulus convection and despite reasonably large amounts of precipitation, the synoptic system does not grow (e.g., Ruprecht and Gray, 1976). Exp. 20, between 15:00 and 40:00 h, seems to simulate such a situation. Here, the propagating convective system is in the dominant motion. Although the convective system formation is a result of the vortex-scale frictional inflow, the vortex scale appears to exert little control on the convection for a period of several tens of hours. Although the convection significantly modifies the vortex, there is no important intensification of the latter. This convection is noncooperative in the CISK sense.

Sensitivity tests with the explicit calculation have shown that this model is capable of discriminating between modes of convection that are cooperative and noncooperative. In

[1]It is emphasized that these results do not eliminate the need for the representation of subgrid convective clouds. They may well, however, mean that far less will be demanded of the subgrid cumulus parameterization than has heretofore been the case.

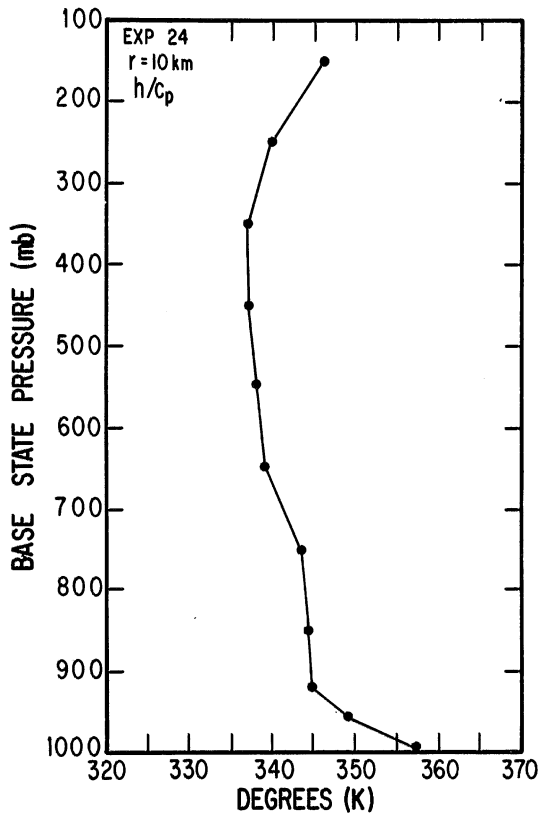

Figure 51.—Vertical cross section of initial moist static energy divided by the specific heat capacity at constant pressure as function of base-state pressure (Exp. 24).

Exp. 24, the only difference from Exp. 20 is an initial state in which the relative humidity is everywhere 100%. This provides for a significant increase of the moist static energy in the middle troposphere (fig. 51) and, thereby, a smaller vertical decrease of moist static energy in the lower troposphere. Figure 52 shows the vertical motion at 5:40 h of this calculation and reveals a deep plume-like convection without downdraft and resembling the type of convection that comprises the eyewall in Exp. 20 (Rosenthal, 1978). This plume does not propagate. However, as the result of gravity waves that are excited by the moist convection, more plumes form. Figures 53 and 54 show the data at 5:55 and 6:15 h and illustrate the development of secondary plumes. Figure 55 shows that plumes are still the dominant mode of convection at 12:00 h.

Some physical insight into the differences between this convection and that found in Exp. 20 can be obtained from figures 56 and 57. These figures show the moist static energy at 5:20 and 5:35 h of Exp. 24. The important fact is that low-level cutoffs of boundary-layer air, and the subsequent formation of low-level stable layers, do not occur here. The cutoff that does occur near 450 mb produces a thin layer of absolute stability in the updraft, but this is at a level where the ambient atmosphere is itself absolutely stable. Presumably, low-level cutoffs do not occur because the compensating subsidence is not as dry (not as low in moist static energy) as in Exp. 20. This plume mode of convection should be more cooperative than the bubble mode, since the plumes are stationary relative to the vortex. Figure 58 shows that the tangential component of the wind already exceeds 20 m s^{-1} at 12:00 h and that the wind is already starting to take on a hurricane-like structure. Speculations of a similar nature, but based on observational data, have been made by Zipser (1971).

In any event, the explicit calculation is capable of differentiating between substantially different modes of moist convection when initial conditions are varied. Figures 59 and 60 show that the calculation is also capable of making this transition within a given numerical experiment as various processes alter the static stability of the system. The plume-like feature (fig. 59) in the

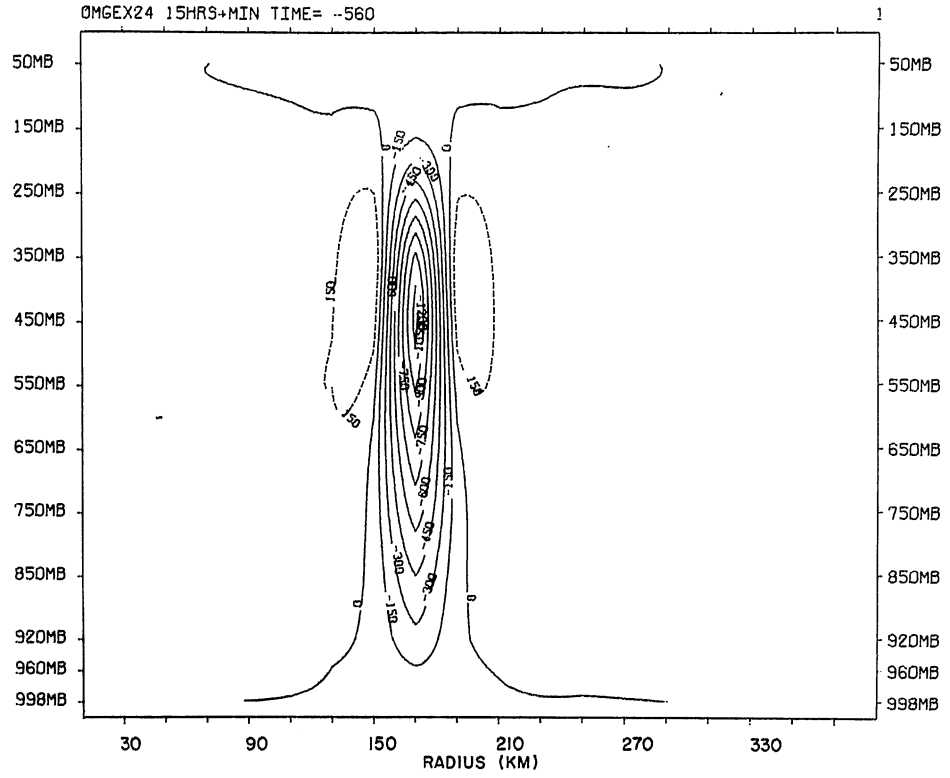

Figure 52.—Vertical cross section of ω at 5:40 h (Exp. 24).

vortex interior at 60:00 h of Exp. 20 is the first evidence (Rosenthal, 1978) of an eyewall feature that can be found in hourly history data. The moist static energy (fig. 60) in the vicinity of this feature more closely resembles that associated with the plumes of Exp. 24 (figs. 56 and 57) than with the earlier intermittent convection found in Exp. 20.

Other sensitivity experiments were run to test the role played by lateral mixing (Eq. 1), the dry convective adjustment and the horizontal resolution. In Exp. 20A, the linear part (C_1) of K_H was suppressed. In comparison with Exp. 20, there were no major changes in either the nature of the early convection or in the hurricane structure. However, the squall line did develop about an hour sooner. In Exp. 27, the total lateral mixing term was suppressed. The early convection was again of the intermittent type with a propagating squall line. The major difference in this stage of the system's development was the formation of secondary propagating convective systems. In Exp. 90, the total lateral mixing was as in Exp. 20, but the dry convective adjustment was suppressed. Again, there were no important differences from Exp. 20 in the mode of the early convection.

In Exp. 91, the horizontal resolution in the uniform portion of the grid was reduced to 10 km. To avoid major recoding, it was necessary to treat a smaller initial vortex and to reduce the computational domain. Again, intermittent convection and a propagating squall line were generated in the early portion of the integration. Surprisingly, however, the system was weaker and did not persist as long as in Exp. 20. At this time, it is not totally clear why, but it appears that the horizontally smaller updrafts were more quickly and effectively diluted by the dry air that came to low levels in the compensating subsidence than was the case for the experiments with 20-km resolution.

6. ACKNOWLEDGMENTS

The author is indebted to John M. Brown, Robert A. Houze, Richard Anthes, Raúl López, Richard Reed, J. M. Fritsch, and several members of the NHRL staff for helpful discussions and reviews of earlier drafts of the manuscript.

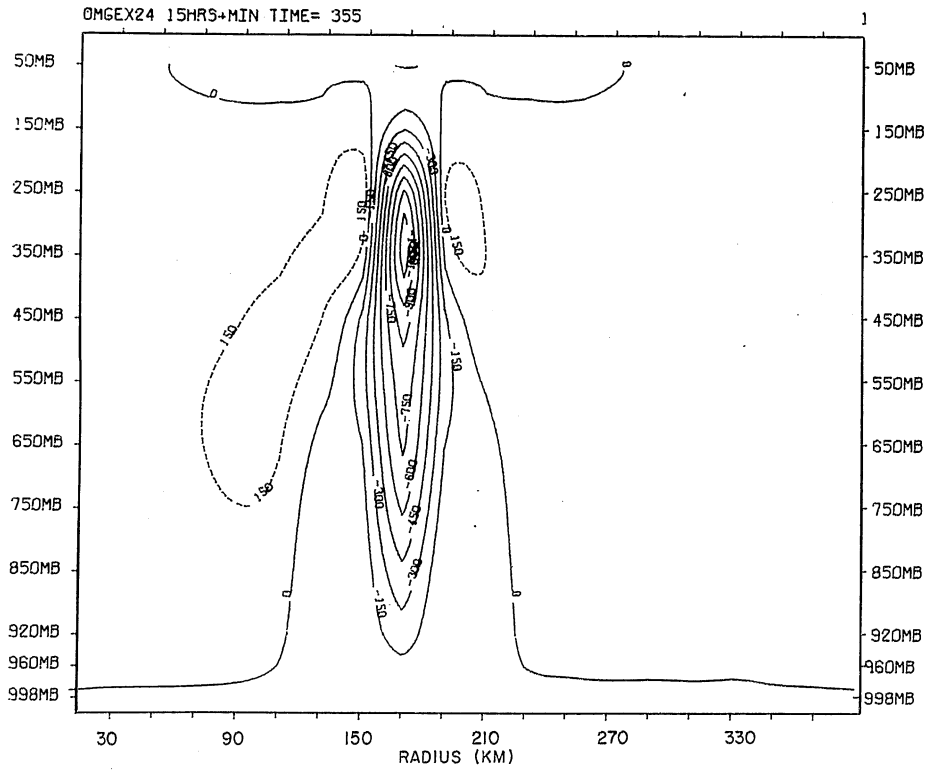

Figure 53.—Vertical cross section of ω at 5:55 h (Exp. 24).

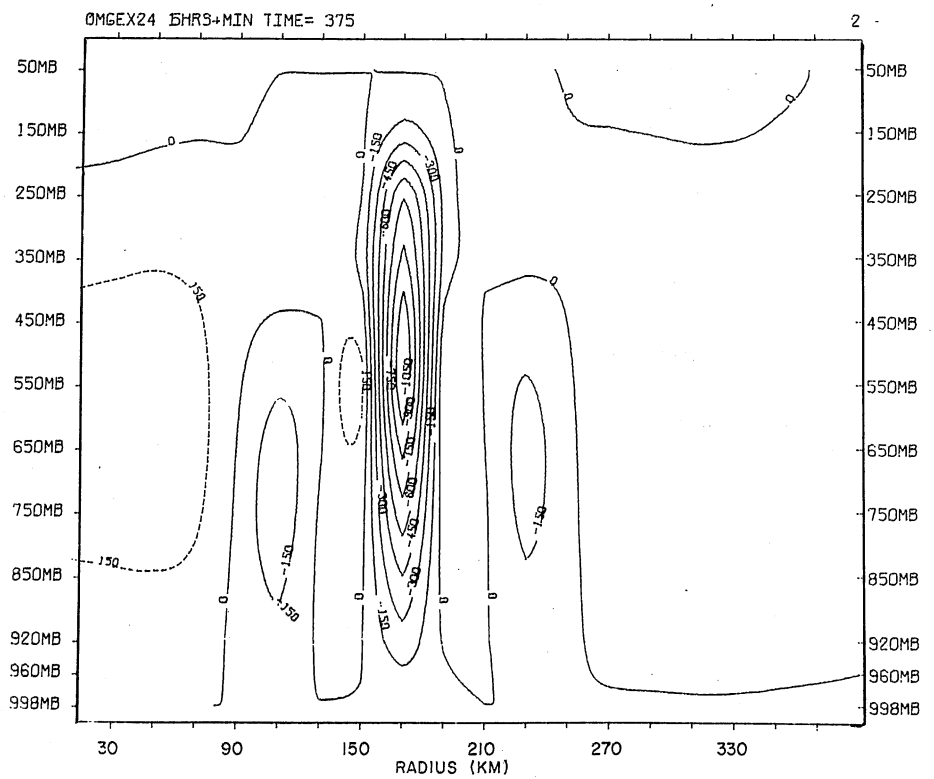

Figure 54.—Vertical cross section of ω at 6:15 h (Exp. 24).

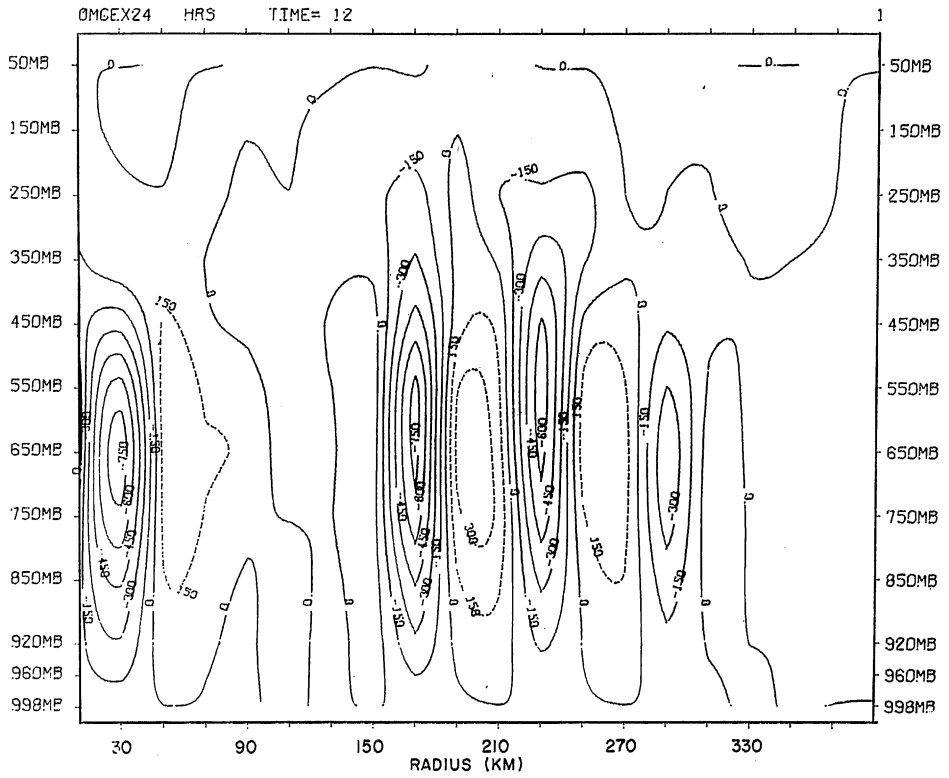

Figure 55.—Vertical cross section of ω at 12:00 h (Exp. 24).

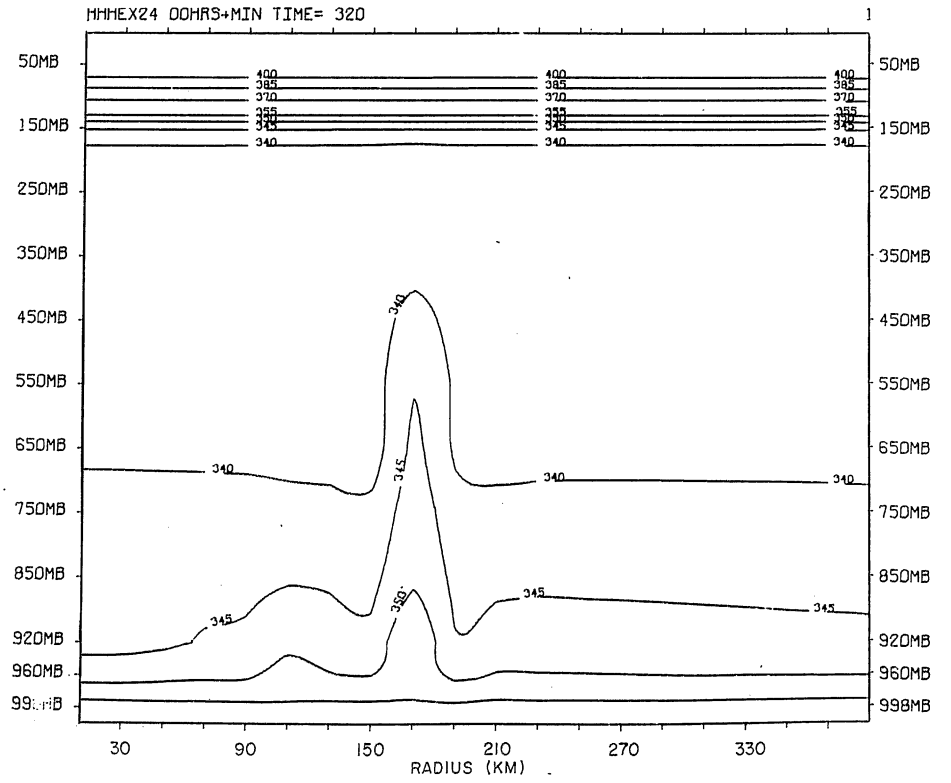

Figure 56.—Vertical cross section of moist static energy at 5:20 h (Exp. 24).

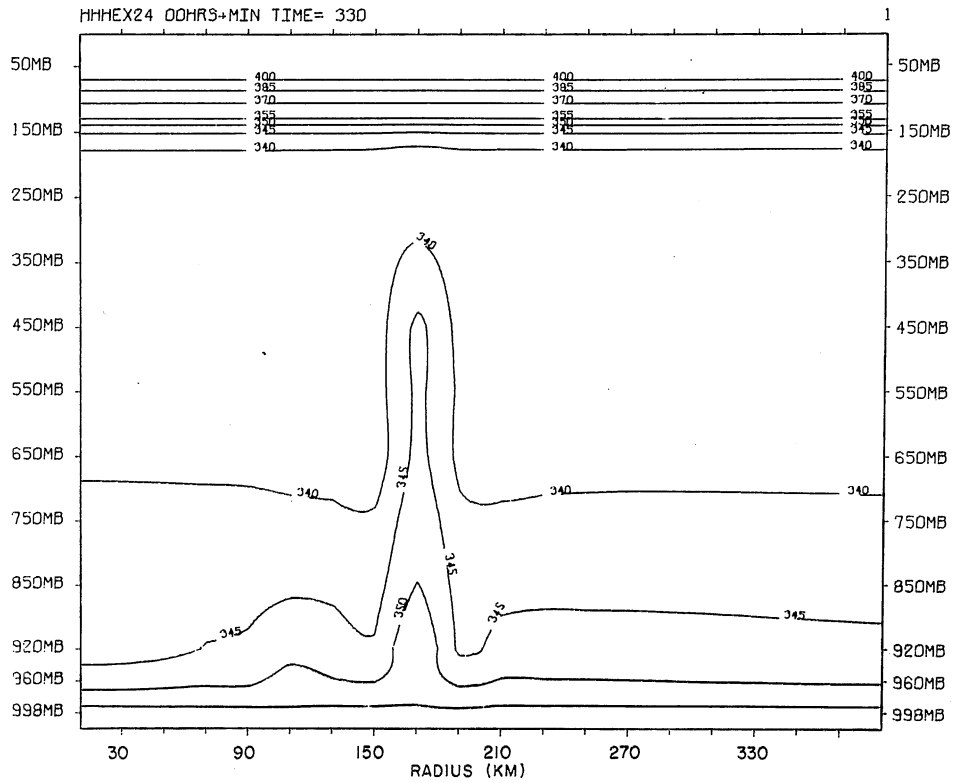

Figure 57.—Vertical cross section of moist static energy at 5:30 h (Exp. 24).

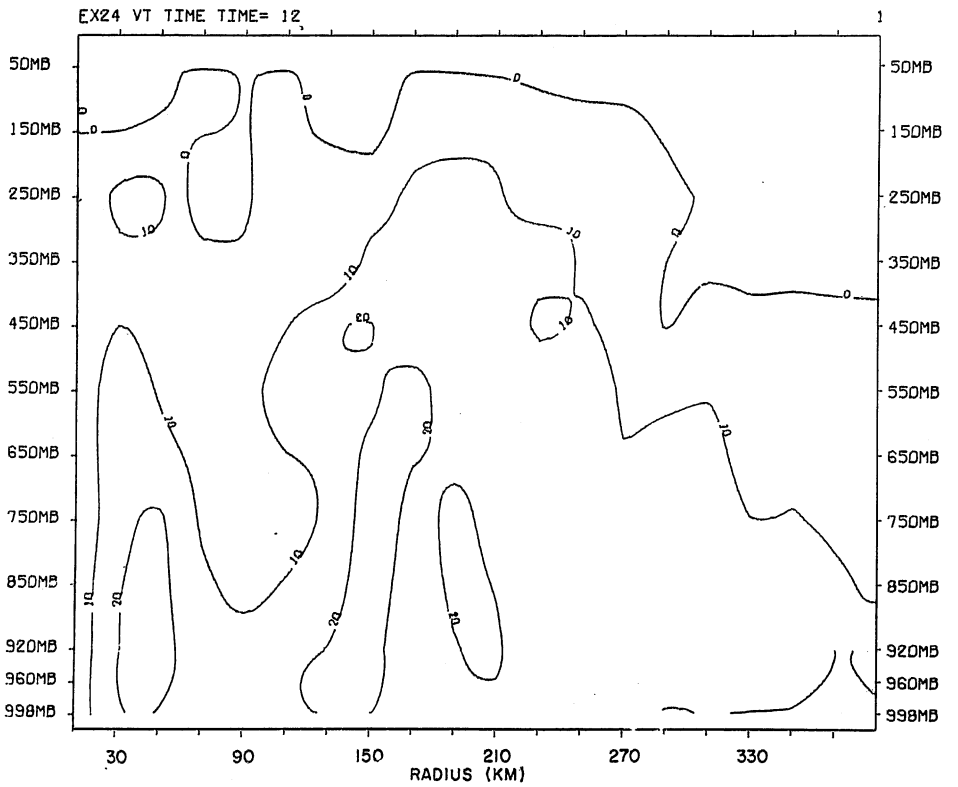

Figure 58.—Vertical cross section of tangential component of wind at 12:00 h (Exp. 24).

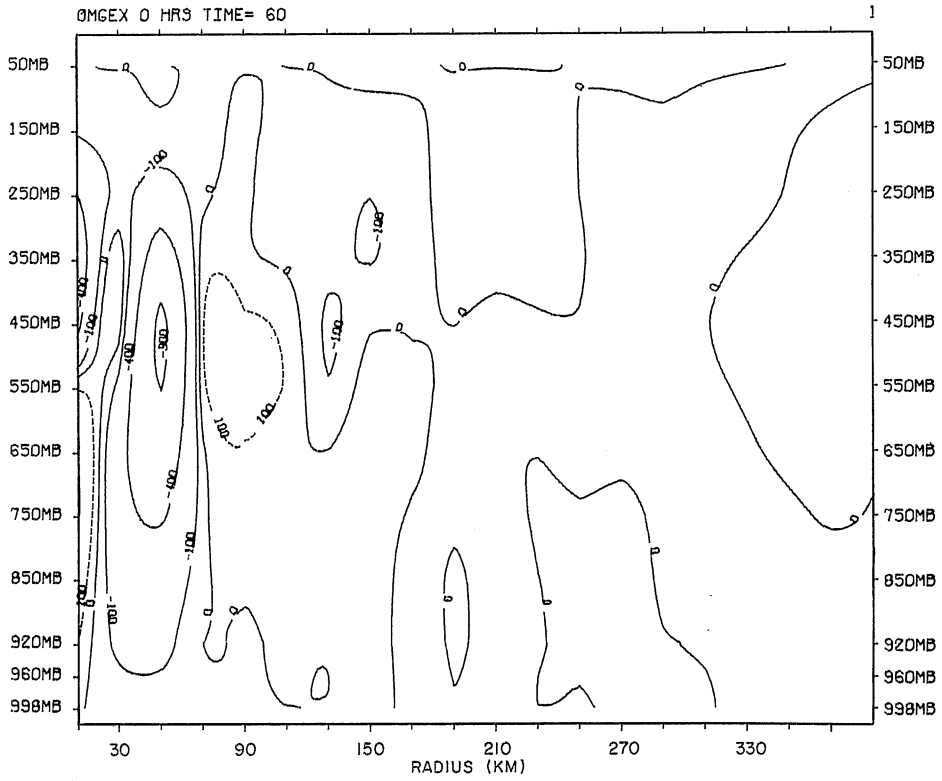

Figure 59.—Vertical cross section of ω at 60:00 h (Exp. 20).

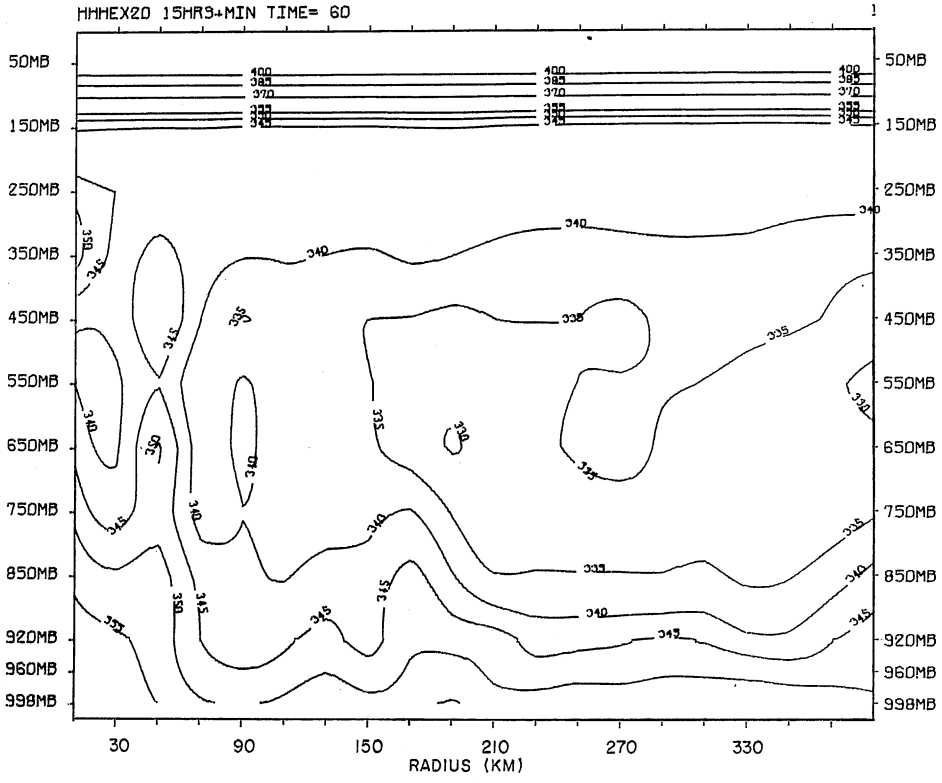

Figure 60.—Vertical cross section of moist static energy at 60:00 h (Exp. 20).

7. REFERENCES

Anthes, R. A. (1972): Development of asymmetries in a three-dimensional numerical model of the tropical cyclone. *Mon. Weather Rev.*, 100, 461–476.

Betts, A. K. (1976): The thermodynamic transformation of the tropical subcloud layer by precipitation downdrafts. *J. Atmos. Sci.*, 33, 1008–1020.

Brown, J. M. (1974): Mesoscale motions induced by cumulus convection: A numerical study. Ph.D. thesis, Massachusetts Institute of Technology, Cambridge, Mass. 206 pp.

Browning, K. A., J. C. Fankhauser, J. P. Chalou, P. J. Eccles, R. G. Strauch, F. H. Merrem, D. J. Musil, E. L. May, and W. R. Sand (1976): Structure of an evolving hailstorm, Part V: Synthesis and implications for hail growth and hail suppression. *Mon. Weather Rev.*, 104, 603–610.

Browning, K. A., and G. B. Foote (1976): Airflow and hail growth in supercell storms and some implications for hail suppression. *Q. J. Roy. Meteorol. Soc.*, 102, 499–533.

Charney, J. G., and A. Eliassen (1964): On the growth of the hurricane depression. *J. Atmos. Sci.*, 21, 68–74.

Estoque, M. A., and C. M. Bhumralkar (1969): The flow over a localized heat source. *Mon. Weather Rev.*, 97, 850–859.

Frank, W. M. (1977): The life-cycle of GATE convective systems. Presented at NCAR GATE Workshop, Boulder, Colo., August 1977. Unpublished manuscript.

Fritsch, J. M. (1975): Cumulus dynamics: Local compensating subsidence and its implications for cumulus parameterization. *Pure Appl. Geophys.*, 113, 851–866.

Hane, C. E. (1973): The squall-line thunderstorm: Numerical experimentation. *J. Atmos. Sci.*, 30, 1672–1690.

Haque, S. M. A. (1952): The initiation of cyclonic circulation in a vertically unstable stagnant air mass. *Q. J. Roy. Meteorol. Soc.*, 78, 394–406.

Houze, R. A. (1976): GATE radar observations of a tropical squall line. *17th Conf. on Radar Meteorol.*, Oct. 26–29, 1976, Seattle, Wash. Preprint, A.M.S., Boston, Mass. 384–389.

Houze, R. A. (1977): Structure and dynamics of a tropical squall-line system. *Mon. Weather Rev.*, 105, 1540–1567.

Hoxit, L. R., C. F. Chappell, and J. M. Fritsch (1976): Formation of mesolows or pressure troughs in advance cumulonimbus clouds. *Mon. Weather Rev.*, 104, 1419–1428.

Jordan, C. L. (1958): Mean soundings for the West Indies area. *J. Meteorol.*, 15, 91–97.

Kasahara, A. (1961): A numerical experiment on the development of a tropical cyclone. *J. Meteorol.*, 18, 259–282.

Kasahara, A. (1962): The development of forced convection caused by the release of latent heat of condensation in a hydrostatic atmosphere. Proc. Int. Symp. Numer. Weather Predict., Tokyo, Nov. 1960, S. Syono, ed., Meteorol. Soc. Japan, 387–404.

Kessler, E. (1969): On the distribution and continuity of water substance in atmospheric circulations. *Meteorol. Monogr.*, 10(32), 1–84.

Kondo, J. (1975): Air-sea bulk transfer coefficient in diabatic conditions. *Boundary Layer Meteorol.*, 9, 91–112.

Kurihara, Y. (1965): On the use of implicit and iterative methods for the time integration of the wave equation. *Mon. Weather Rev.*, 93, 33–46.

Kurihara, Y. (1975): Budget analysis of a tropical cyclone simulated in an axisymmetric numerical model. *J. Atmos. Sci.*, 32, 25–29.

Kurihara, Y., and R. E. Tuleya (1974): Structure of a tropical cyclone developed in a three-dimensional numerical simulation model. *J. Atmos. Sci.*, 31, 893–919.

Lewis, J. M., Y. Ogura, and L. Gidel (1974): Large-scale influences upon the generation of a mesoscale disturbance. *Mon. Weather Rev.*, 102, 545–560.

Lilly, D. K. (1960): On the theory of disturbances in a conditionally unstable atmosphere. *Mon. Weather Rev.*, 88, 1–17.

Lilly, D. K. (1975): Severe storms and storm systems: Scientific background, methods, and critical questions. *Pure Appl. Geophys.*, 133, 713–734.

Ludlam, F. H. (1963): Severe local storms: A review. *Meteorol. Monogr.*, 5(27), 1–32.

Matsuno, T. (1965): Numerical integration of the primitive equations by a simulated backward difference method. *J. Meteorol. Soc. Japan*, 44, 76–84.

Miller, M. J., and A. K. Betts (1977): Traveling convective storms over Venezuela. *Mon. Weather Rev.*, 105, 833–848.

Moncrief, M. W., and J. J. Miller (1976): The dynamics and simulation of tropical cumulonimbus and squall lines. *Q. J. Roy. Meteorol. Soc.*, 102, 373–394.

Moss, M. S., and S. L. Rosenthal (1975): A note on the hydrostatic equation in the NHEML two-dimensional hurricane model. NOAA Tech. Memo. ERL WMPO-26, 14 pp.

Newton, C. W., and J. C. Fankhauser (1975): Movement and propagation of multicellular convective storms. *Pure Appl. Geophys.*, 113, 747–764.

Rosenthal, S. L. (1978): Numerical simulation of tropical cyclone development with latent heat release by the resolvable scales I: Model description and preliminary results. *J. Atmos. Sci.*, 35, 258–271.

Ruprecht, E., and W. M. Gray (1976): Analysis of satellite-observed tropical cloud clusters II.

Thermal, moisture and precipitation. *Tellus*, 28, 414–425.
Schlesinger, R. E. (1973): A numerical model of deep moist convection: Part II. A prototype experiment and variations upon it. *J. Atmos. Sci.*, 30, 1374–1391.
Schlesinger, R. E. (1975): A three-dimensional numerical model of an isolated deep convective cloud: Preliminary results. *J. Atmos. Sci.*, 32, 934–957.
Seguin, W. R., and M. Garstang (1976): Some evidence of the effects of convection on the structure of the tropical subcloud layer. *J. Atmos. Sci.*, 33, 660–666.
Smagorinsky, J. (1963): General circulation experiments with the primitive equations: I. The basic experiment. *Mon. Weather Rev.*, 91, 99–164.
Syōno, S. (1953): On the formation of tropical cyclones. *Tellus*, 5, 179–195.
Syōno, S. (1963): A numerical experiment of the formation of tropical cyclones. Proc. Int. Symp. Numer. Weather Predict., Tokyo, Nov. 1960, S. Syōno, ed., Meteorol. Soc. Japan, 405–418.
Takeda, T. (1971): Numerical simulation of a precipitating convective cloud: The formation of a long-lasting cloud. *J. Atmos. Sci.*, 28, 350–376.
Wilhelmson, R. (1974): The life cycle of a thunderstorm in three dimensions. *J. Atmos. Sci.*, 31, 1629–1651.
Williams, K. T., and W. M. Gray (1973): Statistical analysis of satellite-observed trade wind cloud clusters in the western North Pacific. *Tellus*, 25, 313–336.
Zipser, E. J. (1969): The role of organized unsaturated downdrafts in the structure and rapid decay of an equatorial disturbance. *J. Appl. Meteorol.*, 8, 799–814.
Zipser, E. J. (1971): Internal structure of cloud clusters. GATE Experimental Design Proposal, Interim Scientific and Management Group, Vol. 2, Annex VII, WMO–ICSU, Geneva, 16 pp.
Zipser, E. J. (1977): Mesoscale and convective-scale downdrafts as distinct components of a squall line structure. *Mon. Weather Rev.*, 105, 1568–1589.